www.MaterialsViews.com

ADVANCED MATERIALS
www.advmat.de

Thinning and Shaping Solid Films into Functional and Integrative Nanomembranes

*Gaoshan Huang and Yongfeng Mei**

Conventional solid films on certain substrates play a crucial role in various applications, for example in flat panel displays, silicon technology, and protective coatings. Recently, tremendous attention has been directed toward the thinning and shaping of solids into so-called nanomembranes, offering a unique and fantastic platform for research in nanoscience and nanotechnology. In this Review, a conceptual description of *nanomembranes* is introduced and a series of examples demonstrate their great potential for future applications. The thinning of nanomembranes indeed offers another strategy to fabricate nanomaterials, which can be integrated onto a chip and exhibit valuable properties (e.g. giant persistent photoconductivity and thermoelectric property). Furthermore, the stretching of nanomembranes enables a macroscale route for tuning the physical properties of the membranes at the nanoscale. The process by which nanomembranes release from a substrate presents several approaches to shaping nanomembranes into three-dimensional architectures, such as rolled-up tubes, wrinkles, and the resulting channels, which can provide fascinating applications in electronics, mechanics, fluidics, and photonics. Nanomembranes as a new type of nanomaterial promise to be an attractive direction for nanoresearch.

1. Introduction: from Solids to Nanomembranes

1.1. Concept

Thin solid films are nowadays widely used in various engineering systems (e.g. flat panel displays, Si planar technology, protective coatings etc.), and have meanwhile been widely investigated from the perspectives of both fundamental research and practical applications. Related studies have an important influence on modern materials sciences, microelectronics, optics, biology and so on, which also pave the way for more and more interesting and exciting applications in many fields, especially the interdisciplinary areas such as micro-/nanoelectromechanical systems (MEMS/NEMS) and lab-on-a-chip technology.

The materials themselves can be classified according to their geometrical configurations.[1] Different from bulk solid materials, a structure which is small in one direction compared to its extent in the other two directions is termed a thin solid film.[1] However, it is worth noting that the qualifier “small” is not accurate from a scientific point of view. As a conceptual guide in practical investigations, “small” commonly means that the largest dimensions are at least one or two orders of magnitude greater than the small dimensions. Researchers in the micro-/nanoscience community are interested in thin solid film structures that have special properties and novel applications, otherwise the structures are still considered as bulk-like even though the thickness is much smaller than the planar dimension.

The recent development of nanoscience has given birth to a new concept in the materials family: nanomembranes. The term “nanomembrane” refers to membrane with thickness in the range of one to a few hundred nanometers, and is normally isolated from its environment at both sides (e.g. by air, vacuum or a dissimilar other material). The structures feature sizes between the atomic scale and macro scale and therefore may have properties different from those they exhibit on a purely macro scale due to differences in size and surface properties. For instance, the thinness makes nanomembrane deformable in a much more pronounced way than its bulk counterpart. In addition, with greatly decreasing structural size, electronic properties of solids are altered leading to a significant quantum confinement effect. In these cases, traditional disciplines need to be re-interpreted, often leading to novel and significant applications of nanotechnology. These factors make the investigations related to nanoscience increasingly attractive. In this Review, we use the term “nanomembrane” to define a group of special films with thicknesses between one to a few hundred nanometers regardless of whether they possess a single-layer or multilayer structure.[2] Obviously, the term “nanomembrane” actually represents a special case of the traditional thin solid film,

---

Prof. G. S. Huang, Prof. Y. F. Mei
Department of Materials Science
Fudan University
Shanghai 200433, China
E-mail: yfm@fudan.edu.cn

Prof. Y. F. Mei
State Key Laboratory of Functional Materials for Informatics
Shanghai Institute of Microsystem and Information Technology
Chinese Academy of Sciences, Shanghai 200050, China

Prof. Y. F. Mei
Key Laboratory for National Defense Science and Technology of
Innovative Micro-Nano Devices and System Technology
Chongqing University
Chongqing 400030, China

DOI: 10.1002/adma.201200574

defined by its extreme thinness. The overlap of these concepts may be confusing since "thin solid film" in some literature may also refer to a film with a thickness of less than a few hundred nanometers. To avoid this confusion, we hereafter consider films with a thickness of less than a few hundred (typically less than 100) nanometers as nanomembranes, and their thicker counterparts as normal thin films. Nanomembranes bridge the gap between nanoobjects and macroscopic objects due to their nanothickness and large lateral dimensions,[2] and may be manipulated without special equipment and observed with the naked eye.[3] **Figure 1** schematically exhibits the nanomembrane family, which are obtained by thinning and shaping bulk materials. The nanomembranes can be manipulated and even released from the substrates to become freestanding. The smaller thickness of nanomembranes makes them easier to shape and be architected to form fascinating planar or three-dimensional structures with various functions. A recent review summarizes the progress of single-crystal semiconductor nanomembranes in the fields of both fundamental study and application in electronics.[2] One may anticipate that more interesting structures and their amazing applications will be derived from nanomembranes of various materials in the future, which forms the basis for this Review.

In this Review, newly explored physical properties and application potentials of shaped artificial nanomembranes, in particular freestanding ones and corresponding two- or three-dimensional architected structures, will be summarized and reviewed. The nanomembranes highlighted here consist of a broad range of materials e.g. semiconductors, oxides, and metals, and correspondingly possess properties and application potentials in different fields, which we believe are of great interest for researchers from many disciplines. For the sake of integrity, regular thin films which have important properties and interesting applications, and which may be further thinned into nanomembranes, will also be briefly introduced.

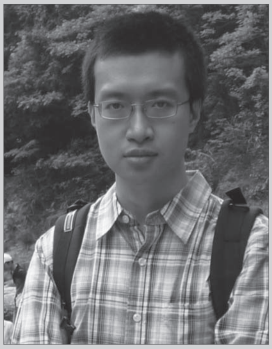

Gaoshan Huang received his Ph. D. in condensed mater physics at the Nanjing University, China in 2007. After graduation, he worked in IFW Dresden, Germany as a guest scientist for two years. Then he moved to IMRE, Singapore as a research engineer. In 2010, he joined the Department of Materials Science, Fudan University, China, as an associate professor. His current research interest is fabrications and characterizations of low-dimensional structures.

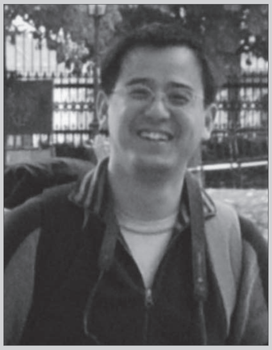

Yongfeng Mei received his PhD at City University of Hong Kong in 2005. After that, he joined the Max Planck Institute for Solid State Research as a post-doctoral researcher. In 2007, he moved to IFW Dresden as a group leader in the Institute for Integrative Nanosciences. His group mainly focused on nanomembranes technology. In 2010, he joined the Department of Materials Science, Fudan University, China as a full professor in materials chemistry and physics. His research interest focuses on the development of novel inorganic nanomembranes.

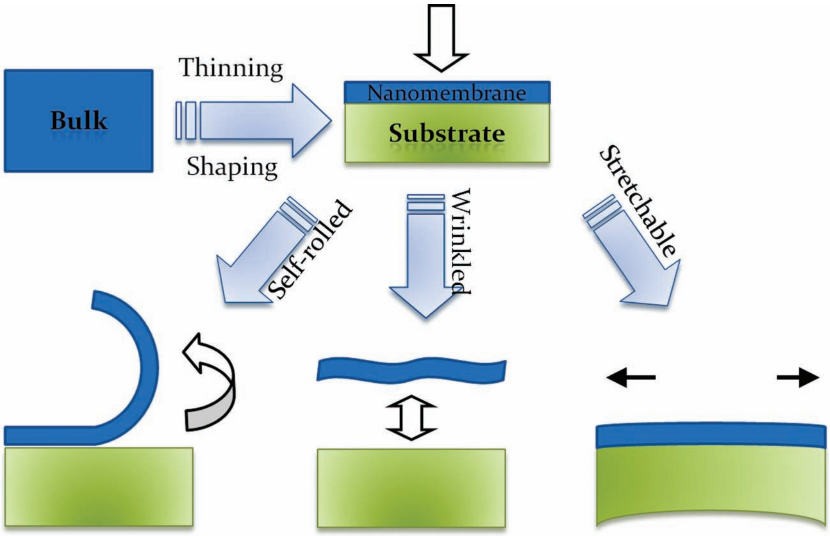

Figure 1. Schematic diagram exhibiting the nanomembrane family. The nanomembranes, obtained by thinning and shaping bulk solid materials, can be manipulated and released from the substrates for various functions. Several three-dimensional structures have already been created and more interesting structures and applications from nanomembranes are expected in the future.

1.2. Technical Notes

The processes used to fabricate thin solid films are normally also applicable to nanomembrane formation, but extra caution must be paid to the thickness monitoring because of the very small thicknesses required.

Physical vapor deposition (PVD) includes a group of common processes used for nanomembrane growth.[1,4,5] The most common PVD processes used by the nanoscience community are evaporation and sputtering. During evaporation, a source is heated by an electron beam, laser, Joule heating, etc and the atoms are thus evaporated. They travel through the reduced background pressure in the chamber and condense on the growth surface. In the sputtering process, ions of the sputtering gas, typically Ar, are accelerated by an applied electric field and bombard the target. The dislodged atoms from the target form a vapor in the chamber and a nanomembrane on the substrate which is connected to the anode in the electric field.[1]

Chemical vapor deposition (CVD) is a different kind of vapor deposition process. A chemical reaction between volatile compounds of the materials in vapor form yields the final desired product which is then deposited onto the substrate. The affordable cost of the equipment and operating expenses, and the ability to controllably create nanomembranes of widely varying stoichiometry are the reasons why CVD processes are widely used to deposit nanomembranes of various materials.

Molecular beam epitaxy (MBE) is a method of depositing single crystals in a high vacuum or ultra-high vacuum, which was invented in the late 1960s at Bell Lab.[6,7] High quality single-crystal film growth can be realized if the surface-diffusion-incorporation time is less than the deposition time of a monolayer.[5] The high quality of the materials deposited is ideal for nanoscience research purposes.

As well as diversified vapor deposition processes, wet chemical depositions have also been used to deposit nanomembranes. For instance, the sol-gel method is adopted for the fabrication of nanomembranes starting from a colloidal solution (sol) that acts as the precursor for an integrated network (gel), which can be dip-coated or spin-coated onto a substrate. The following drying and firing processes remove the solvent from the gel, leading to the formation of a nanomembrane.[8,9] Other wet chemical deposition methods may include hydrothermal/solvothermal synthesis[10–13] and electrochemical deposition.[14]

For organic nanomembranes, researchers use spin-coating[15] or the layer-by-layer assembly method.[16,17]

These are by no means the only processes that can be used though, in fact there are various other approaches (e.g. the Smart-Cut process[18]) that can also be utilized in the fabrication of nanomembranes. Nanomembranes obtained from different methods show abundant different structural, morphological, and crystallographic properties, making nanomembrane fabrication a complex knowledge system in itself.[19] Therefore, experimental parameters for desired products need to be carefully considered since they will strongly influence the fabrication.

1.3. Shaping and Releasing

The fabricated nanomembrane is of a flat, "two-dimensional" geometry attached to the substrate and needs to be shaped into different geometries for further applications. The easiest shaping method is mechanical scratching, which can be done quickly using a diamond cutter or a piece of sand paper.[20] This method can manually pattern the nanomembrane into strips, squares, and rectangles in seconds without the need for specialized equipment, and is widely adopted as a quick test. However, in cases where fabrication of sophisticated structures with small dimensions and high controllability is required, lithography is a must. In fact, lithography also provides the possibility of highly parallel fabrication of integrative devices in a reproducible manner, which is becoming one of the most significant advantages of nanomembrane technology.

Lithography, including photo-lithography and e-beam-lithography, is widely used in the microelectronics industry to transfer a layout pattern onto the surface of a substrate. Generally, photolithography is capable of producing fine structures with a high throughput since patterns on the photomask can be transferred simultaneously, while ebeam-lithography is time-consuming and normally used to fabricate even finer structures because the diffraction limit of the e-beam is much smaller than that of the ultraviolet radiation. At the beginning of the lithography process, a resist layer is coated on the to-be-patterned nanomembrane, and the pattern will then be created on the resist layer by an exposure-development procedure.[1,21] To further transfer the pattern to the nanomembrane underneath, reactive ion etching (RIE) or wet-chemical etching is adopted. The RIE process uses reactive plasma to remove material it contacts. High-energy ions from the gas plasma produced by an electromagnetic field attack the wafer surface and react with it. Both chemical reaction and physical etching from ions with high kinetic energy provide good anisotropic etching behavior and produce excellent vertical sidewalls perpendicular to the etching front.[21] In some cases, wet-chemical etching may be used because it is cheap and convenient. For instance, GaAs or $In_xGa_{1-x}As$ nanomembranes are normally shaped using HBr solution.[22] However, wet-chemical etching may cause severe undercutting beneath the nanomembrane and in certain cases deteriorate the pre-defined shape and is therefore not always suitable.

It is not always necessary to prepare a resist layer on the top to shape a nanomembrane, in fact the resist pattern can be prepared prior to nanomembrane deposition. This technique is known as the lift-off process, which is an additive technique, as opposed to the previous etching process. After the inverse resist pattern is fabricated on the substrate, the deposited material can reach the surface of the substrate in those regions where the substrate is not covered by resist. When the resist layer is washed away, the material on the resist is also lifted-off removed, and the shaped nanomembrane remains in the regions previously without resist layer.[23,24] However, it is worth noting that most resist cannot survive high temperature processes, and therefore is not applied to the deposition where high temperatures are required.

Nanomembranes prepared by the aforementioned methods normally need to be supported by bulk substrates, and this attachment may disturb the property characterization of the nanomembrane itself. More importantly, to architect three-dimensional structures using nanomembranes, researchers must first release the nanomembrane from the substrate. The solution is to insert a sacrificial layer between the nanomembrane and the substrate. In fact the sacrificial layer can even be the top layer of the substrate itself. The sacrificial layer is then chemically removed by lateral etching, using the corresponding etchant. The nanomembrane above then loses support and becomes freestanding. The key in the releasing process is the high etching selectivity of the etchant between the sacrificial layer and the nanomembrane itself and this therefore limits the selection of materials that can be used in preparing freestanding nanomembranes. Here, we summarize several typical nanomembrane systems and corresponding etchants used for release. During the process, the temperature and the concentration of the etchant may have an important influence on the etching rate and even the etching selectivity, and therefore, these factors should be carefully considered before experimentation.

1. Si on insulator (SOI)-based systems. Typical SOI substrate consists of a thin Si nanomembrane on a SiO_2 (insulator) layer.[25] It is worth noting that the SOI technology itself is also a method to fabricate Si nanomembranes. Researchers can also deposit other materials on the topmost Si nanomembrane to make nanomembranes with multi-layer structures. For instance, a diamond-like-carbon layer has been deposited using acetylene plasma to obtain a Si/C bi-layer nanomembrane.[20] To release the nanomembrane from the SOI substrate, researchers normally remove the SiO_2 sacrificial layer using an HF solution at room temperature. 49% HF solution shows good etching selectivity in removing SiO_2, whilst keeping the Si or C layer intact to form a freestanding nanomembrane.[20,26]
2. An NH_4OH solution can effectively etch away an undoped Si layer while the etching rate of a heavily B-doped Si layer is much smaller. It is found that the etching rate of Si with a B concentration of 10^{20} cm^{-3} is 1/8000 that of undoped Si.[21] The etching rate of SiGe in NH_4OH solution is even smaller.[21,27] Therefore, an undoped Si layer is used as a sacrificial layer to release heavily doped Si or a heavily doped Si/SiGe bi-layer nanomembrane.[28–32]
3. Another etchant used to release nanomembranes of group IV semiconductor material is H_2O_2 solution, which can remove a Ge sacrificial layer at 90°C to release a top Si or SiGe nanomembrane.[33–35]
4. In the research concerning group III-V semiconductor materials, $GaAs/In_xGa_{1-x}As$ bi-layer nanomembranes can be fabricated on an AlAs sacrificial layer by using the MBE method on GaAs bulk substrate. In this case, a dilute HF solution at room temperature is found to be a good etchant to selectively etch away AlAs, releasing a $GaAs/In_xGa_{1-x}As$ nanomembrane.[28,33,35,36]
5. Other material systems and corresponding etchants that could permit the formation of freestanding nanomembranes have also been reported. For instance, $Al_xGa_{1-x}As$ was released by using an XeF_2 gaseous etchant to remove the Ge sacrificial layer;[37] a SiO_2 sacrificial layer was removed using HF vapor while the top metal and Si were hardly attacked;[38] and Al can be etched in a mixture solution of H_3PO_4 and HNO_3[39] or KOH-based etchant[40] to obtain a metal nanomembrane.[40] In fact, although it is impossible to list all the materials and their combinations for nanomembrane release, we should stress that researchers do have a lot of options. For this chemical etching step, the experiences from conventional integrated circuit processing could be used as good references.[41]

Obviously, the requirement of high etching selectivity makes the release of some nanomembranes difficult, hindering further investigation. Moreover, to architect three-dimensional structures using freestanding nanomembranes, researchers must first shape the nanomembrane and then release it from substrate. Is it possible to conveniently simplify the procedure by shaping the nanomembrane while simultaneously releasing it? Recently, we developed a new method adopting a photoresist layer as sacrificial layer. As shown in **Figure 2**, the photoresist layer is shaped into a pre-defined geometry using traditional photo-lithography.[42,43] In this case, tilted deposition must be used in vapor deposition processes such as e-beam or thermal evaporation as well as sputtering deposition, as outlined in the diagram. In such cases a narrow gap remains open after deposition at the far end of the patterned photoresist layer due to the ballistic shadow effect that always occurs during glancing angle deposition.[44–46] In the next step, an organic solvent (acetone in most cases) can enter through this gap and removes the sacrificial photoresist layer from one side, leaving the topmost nanomembrane freestanding.[42,43] Obviously, the processes of shaping and releasing the nanomembrane are finished simultaneously since the freestanding nanomembrane accurately duplicates the geometry of the photoresist pattern underneath. Meanwhile, the connection between the freestanding and attached parts at the edge of the photoresist pattern (see Figure 2) provides an easy way to fix the freestanding nanomembrane onto the substrate, offering great convenience for the nanodevices' integration onto a chip. Another important advantage of this approach is that the organic solvents used are able to etch a photoresist sacrificial layer over almost any inorganic material with practically 100% selectivity. Therefore, limitations regarding the selection of materials are largely exempted and freestanding nanomembranes constructed from a range of inorganic materials and their combinations can in principle be prepared using this approach (see section 5.3 for more details).

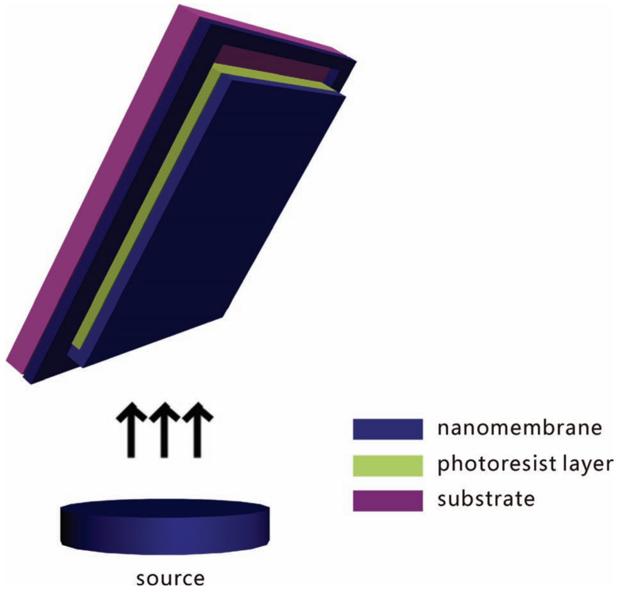

Figure 2. Shaping and releasing of nanomembranes in one step. Patterned photoresist layer is used as a sacrificial layer, and the nanomembrane is deposited by glancing angle deposition which leaves a narrow gap at the far end of the patterned photoresist layer due to the ballistic shadow effect.

2. Ultra-thin Nanomembranes

As we discussed before, nanomembranes from various materials can be obtained using different approaches, and may have unique properties due to their extremely small thickness. In this part, we will discuss one important kind of nanomembrane: ultra-thin nanomembranes, and their novel properties as well as potential applications. These properties are intimately connected with the small thickness of the nanomembranes and therefore cannot be observed in thicker nanomembranes/films or in bulk cases. For the sake of clarity, we shall refer to these kinds of nanomembranes as ultra-thin nanomembranes from now on.

2.1. Ultra-thin Si nanomembranes

Si is an abundant element, second only to oxygen, in the Earth's crust. It is biocompatible and widely used in the microelectronics industry.[47] Single-crystal Si as an ideal model system with high technological value has attracted a lot of interest. Naturally, Si in the form of a nanomembrane, which keeps its original crystal structure even in such small thicknesses, has been intensively investigated.[47] The research group lead by Prof. M. G. Lagally in the University of Wisconsin-Madison has carried out several pioneer works related to ultra-thin Si nanomembranes,[21,47,48] and unique mechanical and electronic properties were also explored in regular Si nanomembranes.[49–55] The results not only provide Si research with a new life but also have benefits from the perspective of fabricating electronic and even opto-electronic devices for practical applications. Furthermore, future studies related to other semiconductor nanomembranes may also benefit from the outcome of the Si nanomembrane investigations. For instance, ultra-thin III-V semiconductor nanomembranes have recently been fabricated on a Si/SiO$_2$ substrate via a so-called "XOI" technology (in contrast to SOI technology), which possesses excellent electronic device performance.[56]

2.1.1. Electronic Transport in Ultra-thin Si Nanomembranes

When the nanomembrane is very thin, the assumption that an infinite number of atoms contributes to its physical properties no longer applies, giving birth to new properties.[57–59] The electrical conductivity of Si nanomembranes could be quite different from their bulk counterparts because of the interface effect.[49,60,61] To understand this, the doping of Si nanomembranes needs to be considered. With decreasing nanomembrane thickness, the total number of dopants becomes smaller, and the sheet resistance should increase. The total number of the dopants in 1 cm^2 of 100 nm thick Si nanomembrane is 10^{10} at a typical doping level of 10^{15} cm^{-3}.[49,60,61] For Si nanomembranes in an SOI structure, the interface states are of the order of 10^{11} cm^{-2} at each Si/SiO$_2$ interface mainly in the forms of Si dangling bonds which can trap charge, depleting the Si of mobile charge carriers.[49,60] Therefore, a 100 nm thick Si nanomembrane should behave as if it was intrinsic at room temperature. Experimental observation demonstrated that for a 150 nm thick 10^{15} cm^{-3} doped Si nanomembrane with native oxide, the resistance is greater than the nominal value calculated without considering interface states (see **Figure 3**a). If the thickness is further decreased to less than 20 nm, the resistance approaches that of intrinsic Si (see Figure 3b).[49] The conductivity is therefore determined by competition between the interface trap and dopant.[49]

Obviously, the conductivity can easily be tuned intentionally by manipulating the interface traps. For a Si(001) surface with a 2 × 1 reconstruction, the density of dangling bonds on the surface is minimized. Calculation shows that charge transfer inside the tilted dimers creates π^* and π bands,[49,60,61] and electrons are easier to thermally excite across the gap from the bulk valence band to the surface π^* band (0.35–0.6 eV) leaving holes in the valence band (see Figure 3c). Both electrons on the surface and holes in the nanomembrane can now contribute to the conductivity. This surface doping solves the problem of dopant fluctuation in nanodevices[62] and the carrier mobility can be improved through decreased scattering of the bulk dopants.[61]

More experimental works have recently been done by the same group.[63–65] It was found that a 2 × 1 reconstruction is experimentally difficult to obtain. However, H-terminated Si surfaces can be easily fabricated by HF etching, which leaves a nominally H-terminated Si surface and trace amounts of OH and F.[65–68] Electric conductivity measurements have demonstrated a very large reduction in the sheet resistance of ultra-thin nanomembranes exposed to HF solution. For thicker nanomembranes/films of high doping concentrations (>10^{15} cm^{-3}), bulk behavior was observed. Meanwhile, Hall measurements revealed that the HF treatment produces an inversion from a nominally p-type nanomembrane to an n-type nanomembrane,

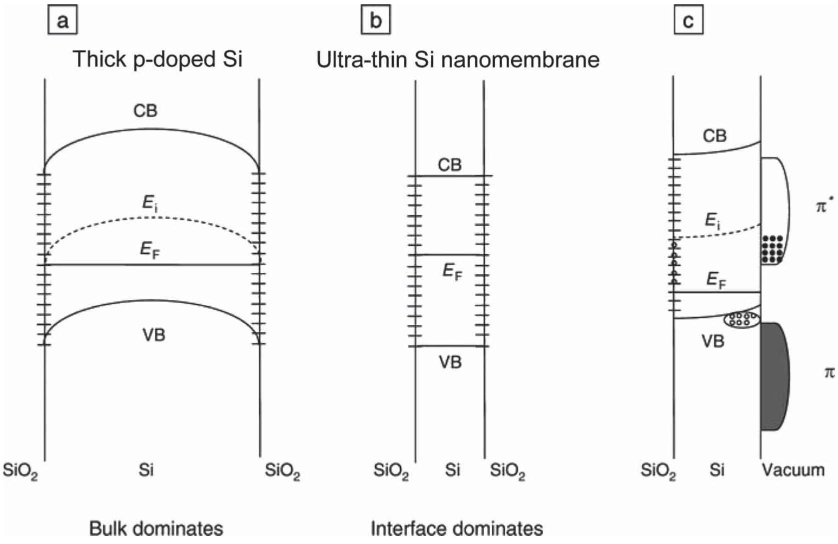

Figure 3. (a) Band structures of Si nanomembranes. (a) In thick p-doped Si nanomembranes, the bulk dominates the band structure. (b) In ultra-thin Si nanomembrane, the interface states trap and deplete carriers, making the ultra-thin nanomembrane intrinsic. (c) Surface dimer reconstruction creates π^* and π bands allowing excitation of electrons from the bulk valence band (VB) to the surface π^* band, which increase the conductivity. Adapted with permission from ref. [49].

which means the conductivity is due to electrons even though the material itself is nominally p-type.[63,65] The observations were considered to be associated with band bending in the near surface region after HF treatment.[63,69–71] H-terminated ultra-thin Si nanomembranes can also be fabricated using vacuum hydrogenation, where surfaces cleaned in an ultrahigh vacuum are dosed with pure hydrogen.[66,72] The conductivity behavior of the Si nanomembrane treated in this way is quite different from the HF-treated one: HF treatment leads to a drop in resistance of three orders of magnitude while vacuum hydrogenation produces a two orders of magnitude drop.[66] The difference was thought to be due to residual species (e.g. OH and F) on the surface and their chemical reaction with time.[66–68] The hydrogenation of both approaches is found to be reversible, and a difference was noted again.[63,65] The resistance of ultra-thin Si nanomembranes treated by HF increases faster than the counterpart treated with vacuum hydrogenation, implying a much better surface chemical passivation of vacuum hydrogenation, and therefore, the HF-treated surface is much more sensitive to re-oxidation.[65] It is worth noting that similar results were also reported in research on bulk Si where surface effects have little influence. The ultra-thin Si nanomembrane effectively isolates the surface from the bulk, inducing a significant change of the Fermi level. In this case, the electronic transport properties are dominated by the surface state.[63,65]

In fact the transport properties can be influenced by many other factors. Detailed investigation has shown that the surface oxide or the free-surface termination may serve as a potential barrier, which effectively confines the conduction band electrons in an ultra-thin Si membrane, making the membrane a quantum well. The long-range order in the direction perpendicular to the surface of the nanomembrane results in the formation of two-dimensional sub-bands in each of the 6-fold degenerate valleys of bulk Si (Δ_6), and the confinement in this direction splits the degeneracy of Δ_6 into 2-fold-degenerate Δ_2 valleys and 4-fold-degenerate Δ_4 valleys. Correspondingly, the conduction band minimum is effectively shifted upward by the ground-sub-band energy.[64] This shift is sensitive to the strain of the membrane.[73] The strain originating from the Si/oxide interface can lead to strain as high as 0.3%,[74] which contributes at most 15 meV to the splitting of Δ_6 for the ultra-thin nanomembrane.[75] In addition, even very small surface roughness was experimentally and theoretically found to be able to blur or smooth out the nominally step-like features in the density of state,[64] suggesting remarkable conductivity variation resulting from the physical and chemical tuning of surface conditions of ultra-thin Si nanomembranes.

2.1.2. Novel Opto-electronic Properties

A giant persistent photoconductivity (PPC) from rough Si nanomembranes was recently revealed.[76] In the study, metal-oxide-semiconductor field-effect transistors (MOSFET) were fabricated on an ultra-thin Si nanomembrane of 27 nm, where patterned Cr/Au films were used as contacts. Besides the original smooth Si nanomembranes, rough Si nanomembranes were prepared by chemical etching in a 20 wt% KOH solution and a thin Cr film was adopted as a mask. The thin Cr film itself is semipermeable and the etching solution could penetrate through the Cr mask and slightly etch the underlying Si nanomembrane.[76] **Figures** 4a and 4b show the normalized current (I_{DS}, divided by the channel width) versus bias voltage (V_{DS}) curves of the rough and smooth Si nanomembranes probed in the dark and under light illumination respectively. For $V_{DS}<0$, the I_{DS}-V_{DS} characteristics in the dark and under light illumination are similar in both samples, while for $V_{DS}>0$, the difference is noticeable. In the rough Si nanomembrane, the current across the channel is below 0.03 μA/μm in the dark, but increases rapidly to 10.3 μA/μm (V_{DS} = 20 V) under light illumination, while in the smooth Si nanomembrane, the device exhibits a slight, commonly observed photoresponse upon illumination. These results indicate that roughening the surfaces suppresses carrier transport in a Si nanomembrane with positive bias voltages while this suppression can be overcome by illumination. Moreover, Figure 4c shows that the high conductive state activated by lighting persists for a long time (in the order of days) after the light source is removed. As the device is exposed to light at V_{DS} = 20 V and V_G = 2 V, the current across the rough Si channel jumps from 0.01 to 9 μA/μm and then decreases

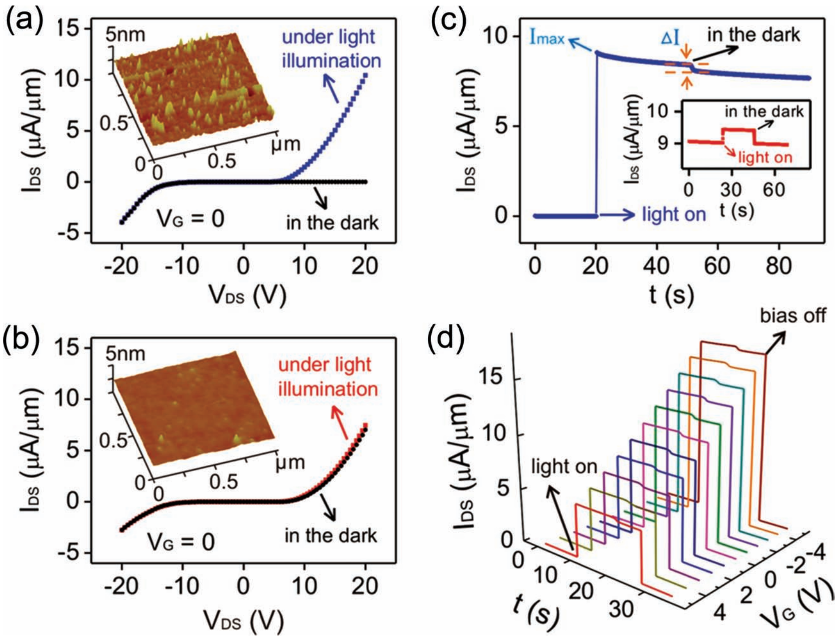

Figure 4. (a) I_{DS}-V_{DS} properties of the rough Si nanomembrane in the dark and under light illumination. The inset shows an atomic force microscopy image of the rough Si nanomembrane. (b) I_{DS}-V_{DS} properties of the smooth Si nanomembrane in the dark and under light illumination. The inset shows an atomic force microscopy image of the smooth Si nanomembrane. (c) Typical PPC results at V_{DS} = 20 V and V_G = 2 V. The inset shows the normal photoresponse of a smooth Si nanomembrane. (d) PPC results at V_{DS} = 20 V, measured at different gate voltages. From left to right, V_G decreases from 5 to –5 V at steps of 1 V. Reproduced with permission from ref. [76]. Copyright 2009 American Chemical Society.

gradually, fitting well with $\ln(I/I_0) \propto -(t/\tau)\beta$ with $\beta \approx 0.59$ and τ in the order of one day or more, where I is the current, I_0 is the maximal current after light illumination, t is the time, τ is the characteristic time constant for the decay of the photocurrent, and β is the decay exponent. The value of τ in rough ultra-thin Si nanomembranes is much higher than those in other Si-based materials.[77] On the other hand, the photoresponse of the smooth Si nanomembrane exhibits usual behaviors, as shown in the inset of Figure 4c. The persistent photocurrent of the rough Si nanomembrane can be adjusted by gate voltages (Figure 4d) and can be turned off by removing the bias voltage (or by applying a large positive gate voltage afterward). The phenomenon that current decreases after light exposure with increasing gate voltage indicates hole transport in the rough Si nanomembrane.[78] PPC effect has been mostly observed in III-V and II-VI semiconductor materials due to insufficient crystalline perfection and has been closely related to deep defect levels.[79,80] The models are not applicable for ultra-thin single-crystal Si nanomembranes. It is considered that the presence of many ridges and valleys compared to the original smooth surface (see insets in Figures 4a and 4b) generates barriers for holes and immobilizes them. Light illumination can effectively activate the confined holes and thus induce the observed PPC effect.

The study also noticed a formation of Schottky contacts between metal and ultra-thin Si nanomembranes.[76] In fact, this is common in nanostructures and the contacts may play a critical role in their electrical properties.[81–83] At the metal-Si contact, the metal's electron wave function decays into the Si nanomembrane, leading to the formation of a depletion layer on the Si side of the interface.[84] Such an electron wave function decay is expected to be sensitive to the properties of the nanomembrane. The control of homogeneity is still challenging in SOI technology,[85] and it has been reported that both Si thickness and strain substantially affect the Schottky barrier height of metal-Si contacts.[86] In SOI-based MOSFET with a channel length of 10–20 μm, it is reasonable to assume that the thickness fluctuations and strains of the nanomembrane at the source and drain areas are different, leading to different band bending at the contacts even if the contacts are made of the same metal. The effect introduced by the difference of the band bending at the source and drain contacts can be well manipulated by gate bias[87] to produce a lateral voltage. With the influence of this lateral voltage, the photovoltaic effect emerges as the devices are excited by local laser illumination at appropriate gate voltages, when the excess carriers excited by illumination are separated by the built-in electric field to produce the photocurrent.[88] This experiment work opens alternative paths for the fabrication of novel nanooptoelectronic devices.

2.1.3. Thermo-electric Properties

Thermo-electric materials are useful in energy-related applications and in the cooling of integrated circuits.[89,90] Investigations indicate that nanomaterials or nanostructures can effectively enhance the Seebeck coefficient and suppress the thermal conductivity.[91,92] However, bulk Si is never considered to be a thermo-electric material due to its high lattice thermal conductivity of ~150 W/m·K.[93–95] By thinning the Si into a nanomembrane, the thermal conductivity can be remarkably reduced, with values reported as low as ~50 W/m·K for ultra-thin Si nanomembranes at room temperature,[93,94] which is orientation dependent.[95] Further reduction in thermal conductivity of the Si nanomembrane can be achieved by creating a high density nanoscopic holes array.[93,94] For instance, a holes array with a pitch of 55 nm causes the thermal conductivity to decrease to ~2 W/m·K, and a clear trend of thermal conductivity reduction as a function of pitch size was observed.[93] The experiment regarding temperature dependent thermal conductivity at low-temperature regions revealed that the geometry of the holes array is quite important in suppressing thermal conductivity.[93] Specifically, when the distance of adjacent holes is smaller than phonon mean free path (MFP, >25 nm for thermal phonon),[96] the holes act as Bragg reflectors. The periodicity of the holes array modifies the phonon band structure by reducing the Brillouin zone and flattening the band, which leads to a decrease in the phonon group velocity,[94] and thus the phonon is "trapped". As a consequence, a local negative temperature gradient opposing the linear temperature gradient along a free channel is created and the thermal conductivity is found to decrease.[93] Meanwhile the electron MFP for highly doped silicon is smaller (~1–10 nm) and thus should not be significantly affected.[93] The Si nanomembrane with nanoholes array was reported to have a ZT value of ~0.4 at room temperature, comparable with the best value recorded in silicon nanowire systems.[93] Optimization in the geometry of the holes array and surface passivation may further promote the thermo-electric properties of the ultra-thin Si nanomembrane-based structures for applications e.g. in on-chip thermal management.[93]

2.2. Freestanding Composite Ultra-thin Nanomembranes

2.2.1. Flexibility and Robustness

For many applications,[97,98] ultra-thin freestanding nanomembranes must combine two characteristics: nanometer thicknesses and macroscopic overall sizes, which are traditionally incompatible. To satisfy these requirements, the obtained nanomembranes must be robust, flexible, and uniform.[99] Some polymers are found to possess such properties, e.g. 20 nm thick epoxy resin nanomembranes prepared using spin coating.[99] The existence of a densely cross-linked structure within the ultra-thin matrix is the key element for the strength of the nanomembrane.[99,100] In principle, most polymers are too soft to form giant ultra-thin nanomembranes. On the other hand, inorganic materials are relatively brittle. In order to achieve both flexibility and robustness, one option is to combine the advantages of organic and inorganic materials, which can be realized at different levels: physical mixing[101,102] and chemical hybridization.[103–106] The robustness of the freestanding nanomembrane can be remarkably improved through hybridization via covalent bonding of organic and inorganic materials.[105,106] Ultra-thin organic-inorganic hybrid nanomembranes with an interpenetrating network structure consisting of polymer and silica, zirconia, or titania have been reported in literature.[105,106] The thickness was found to be constant with an accuracy of 10% over the whole film, with the surface roughness within 2.5 nm, demonstrating good uniformity.[106] The nanomembranes are very flexible and can easily be folded into small shapes. The aspiration of a 16 cm^2 nanomembrane into a micropipette with a tip diameter of approximately 320 μm has been observed.[106] It is worth noting that the size of the micropipette hole is 30 000 times smaller than the size of the nanomembrane, and therefore the aspiration process is believed to be due to the extreme thinness and flexibility of the nanomembrane. Meanwhile, the hybrid nanomembrane has an ultimate tensile stress σ = 105 MPa and an ultimate tensile strain ε = 2.6, clearly indicating the robustness of the hybrid nanomembrane.[106]

Besides the traditional applications of this kind of flexible nanomembrane,[97,98] the flexible ultra-thin nanomembrane has recently been used in surface functionalization.[107] The work has demonstrated that manipulation of surface properties can be performed simply by a decal-like transfer of nanomembranes.[107] The flexible and robust ultra-thin nanomembranes have properties necessary for this application: (1) Fabrication of flexible and robust nanomembranes enables a precise transfer on surfaces with variant morphologies; (2) Ultra-thin nanomembranes provide a large contact area, and this provides strong adhesion of the nanomembrane onto the processed surface; (3) The effect of a nanomembrane's physical properties becomes smaller as the thickness decreases, and thus an ultra-thin nanomembrane should be involved only when surface properties rather than bulk physical properties are required.[107]

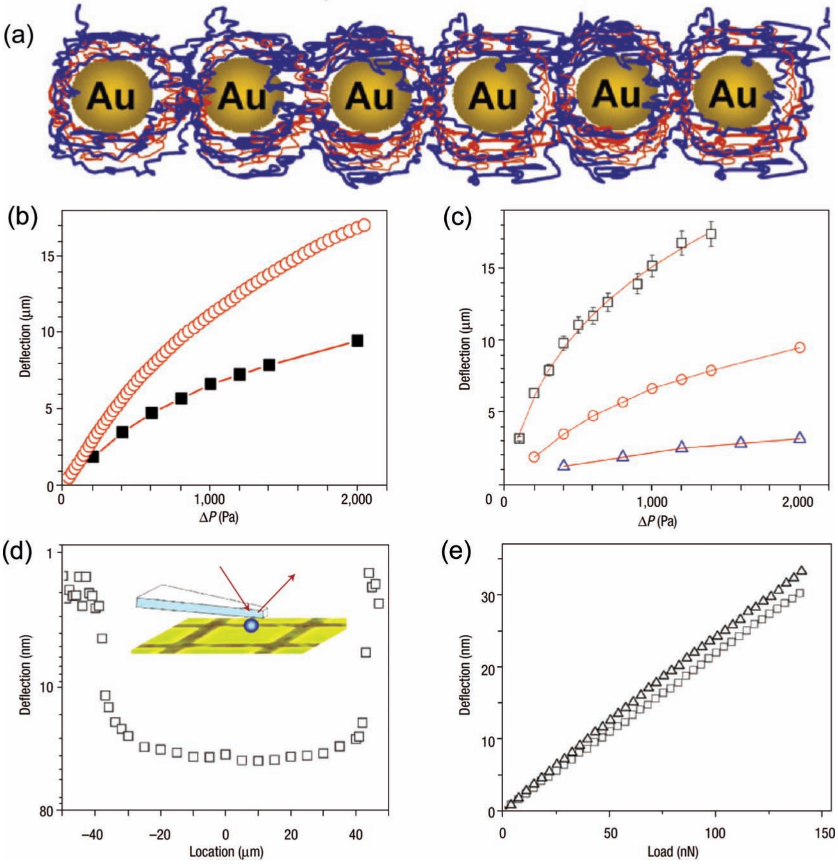

Figure 5. (a) Microstructure of the composite ultra-thin nanomembrane with a gold nanoparticle central layer sandwiched between polymer layers. (b)-(e): Mechanical testing of ultra-thin membranes. (b) Deflection of the composite nanomembrane (filled squares) and polymer nanomembrane without gold nanoparticles (open circles) with pressure (diameter: 400 μm). (c) Deflection of composite nanomembranes with different diameters: 600 μm (squares), 400 μm (circles), and 150 μm (triangles). Solid lines show theoretical fits. (d) Deflection across the composite nanomembrane derived from atomic force microscopy. Inset: a simplified diagram of the experimental setup. (e) Deflection of composite nanomembrane in two different locations. Adapted with permission from ref. [108].

2.2.2. Nanocomposite Ultra-thin Nanomembranes and Optical Properties

Ultra-thin freestanding nanomembranes can be functionalized via incorporation of components with special functions. A typical example is the composite ultra-thin nanomembranes, designed as multilayer nanocomposites fabricated of precisely assembled polymeric monolayers and a metal nanoparticle intralayer with a thickness of 25–70 nm, which are fabricated with molecular precision by time-efficient, spin-assisted layer-by-layer assembly on a sacrificial substrate.[108] The nanomembranes, with nanoscale thickness and macroscopic lateral dimensions, can possess unparalleled sensitivity combined with extreme robustness.[108] A typical nanomembrane is composed of nine bi-layers of poly(allylamine hydrochloride) (PAH) and poly(sodium 4-styrenesulfonate) (PSS) which surrounds a central nanoparticle layer consisting of gold nanoparticles with diameter of ~12.6 nm, and the total thickness is determined to be ~55 nm (see **Figure 5**a). The mechanical behavior of this kind of nanomembrane was investigated using bulge testing, and an optical interferometer was employed to monitor microscopic deflections. As demonstrated in Figures 5b and 5c, the response was clearly nonlinear, and consistent with the theoretical prediction for the large elastic deformation of a circular plate clamped to a stiff edge.[108] The average elastic modulus of 5.7 ± 3.0 GPa and the ultimate strength of these membranes was determined to be 40–100 MPa with the elongation before breaking approaching 1–2%.[108] The existence of a gold nanoparticle intralayer has a remarkable influence on mechanical properties of the nanomembrane: decreasing the content of gold nanoparticles leads to a decrease in the elastic modulus (see Figure 5b), suggesting the existence of the filler toughening mechanism associated with embedded gold nanoparticles.[108,109] The excellent micro-mechanical properties make the nanomembrane a good candidate for use in sensing applications since the deflection of the nanomembrane under a point load of 150 nN reaches 30 nm for a circular membrane with a diameter of 600 μm, and the minimum detected deflection, about 2 nm, was detected under a load of 4 nN (see Figures 5d and 5e).[108] The uniform response shown in Figure 5e is proof of the homogeneity in the composition of the ultra-thin nanomembrane.

It is widely known that Raman scattering can be enhanced by several orders of magnitude in the presence of a noble-metal nanoparticle, a process which is known as surface enhanced Raman spectroscopy (SERS).[110] In the Raman spectrum of the nanomembrane, peaks related to the bending and waging of CH_2 backbone groups and to the in-plane stretching of the side phenyl rings of PSS was observed, and remarkable increase in the peaks' intensity in the region containing gold nanoparticles is considered a proof of SERS, while Raman scattering of free-suspended, purely polymeric nanomembranes showed no strong peaks.[111] The corresponding enhancement factor of the gold nanoparticle in the ultra-thin nanomembrane was calculated to be 10^5, and was ascribed to the unique chain-like arrangement of the gold nanoparticles and the narrow gap (2–8 nm),[111] where the enhancement of the local electromagnetic field near the surface, i.e. excitation of the surface plasmon, leads to SERS. The plasmon resonance from interparticle coupling has been observed and proven experimentally in optical absorption.[112]

With the development of this kind of nanomembrane, nanoparticles other than gold can be incorporated into the composite ultra-thin nanomembrane. For instance, CdSe/ZnS quantum dots and $NaYF_4$:17% Yb, 3% Er nanocrystals have recently been embedded to achieve excellent light emission properties from a freestanding ultrathin nanomembrane.[113,114] Further functionalization of the nanomembranes may have important applications in a new generation of sensing devices.

2.3. Graphenes–Thin to One Atom

Graphene is definitely one of the most popular ultra-thin nanomembranes in the present scientific community. For a long time, researchers believed that true "two-dimensional" materials with thickness of a single atom could not exist, because temperature and quantum fluctuations from atomic vibrations perpendicular to the plane would destroy the two-dimensional structure of this hypothetical material.[115] Nevertheless, in 2004, a group led by A. K. Geim produced such a two-dimensional material by means of mechanical exfoliation of graphite with cellophane tape.[116,117] In this method, graphite plays a key role since this three-dimensional material is itself made of stacked graphene planes bound by van der Waals forces. The developed method permits one to isolate the two-dimensional material on top of a 300-nm-thick SiO_2 layer[115–117] or other substrates.[118] Under the name of graphene, this new material, an allotropic form of carbon, is a monatomic layer of carbon atoms arranged on a honeycomb lattice, and the thickness of the monolayer is determined to be 0.34 nm.[115,119,120] The mechanical exfoliation as a top-down approach produces graphene with the highest quality but the throughput is rather low. Several alternative methods have been explored, each with their own respective drawbacks: chemical exfoliation and stabilization of graphene sheets in solution;[121] growth of graphene directly from organic precursors;[122] in situ catalytic growth on a substrate.[123,124]

The investigations concerning graphene have already exhibited new and interesting physics. For instance, graphene's ambipolar field effect has been observed.[116] Electrons and holes move through the layer with very high mobility and velocities of up to 10^6 m/s.[119,120,125] The quantum Hall effect at room temperature has also been detected.[120,126] In addition to the attractive electric properties, graphene has also demonstrated excellent mechanical properties. An experiment was recently carried out using atomic force microscope nanoindentation, and a second- and the third-order elastic stiffnesses of 340 and –690 N/m respectively was thus derived.[127] The corresponding Young's modulus was calculated to be 1 TPa, implying that graphene is the strongest material ever measured.[127] These new properties of graphene recently disclosed inspire huge interest in fundamental research, and related applications in nanodevices are also very exciting.[128]

3. Bendable and Stretchable Nanomembranes

When solids are thinned into nanomembranes, they become soft and behave like traditional soft matter.[2,47,129] Strain can thus be introduced mechanically, which leads to significant modification of the physical properties.[130] For instance, an interesting investigation recently demonstrated that a stretched Ge nanomembrane is transformed into a direct-bandgap material with strongly enhanced light emission efficiency.[131] Moreover, the research group led by Prof. John A. Rogers in the University of Illinois at Urbana-Champaign has produced very exciting soft devices and integrated systems made from inorganic semiconductor nanomembranes with sophisticated designs, and the obtained systems possess the properties of those made by conventional, rigid wafer-based technologies but with the ability to be stretched, compressed, twisted, and bent.[132–136] Their works suggest that bendable and stretchable nanomembranes not only have important applications in existing devices in flexible form but also open up valuable new possibilities in routine-life applications, especially those related to biology, since most biological applications involve soft and curved surfaces.[135–138] Electronics, sensors, power supply, and communication components made from nanomembranes have been conformally attached onto the surface of the skin by a soft, intimate, and mechanically "invisible" contact.[138] Vision for the development of this aspect extends to wearable computers, personal health monitors, and surgical/diagnostic implements that naturally integrate with human bodies for advanced therapeutic capabilities such as in-situ surveillance and operation.[135,138]

3.1. Flexible and Stretchable Electronics and Opto-electronics

Development of current micro-electronics is based on devices mounted on rigid, brittle, and planar semiconductor substrates. Many researchers believe that the future of electronics and opto-electronics lies in integrated systems without those rigid substrates. This direction, different from its counterpart focused on miniaturization of high speed devices, began more than 15 years ago.[135] The first step towards realizing flexible and bendable electronic devices was to explore new electronic materials. Organics and polymers were the most commonly used materials in that early stage. In order to realize paper-like displays, transistors consisting of semi-conductive polymers were fabricated on bendable plastic substrates.[139,140] The feasibility of this route is based on the flexibility of the materials themselves. Many successes have been achieved in this field,[140–142] but the toxic nature, poor crystalline quality, and low carrier mobility of these pioneer materials limited their applications to low-speed electronics.

Current research is expected to prepare electronic devices that are not only bendable but also stretchable. The devices and the substrates will be able to be compressed, twisted, and deformed in a much more extreme way than is currently possible, and shaped into complex geometries while maintaining their electrical performance and reliability.[135,138] Thinning is a widely used method to improve the bendability and stretchability of such devices because the strain is proportional to the thickness. Traditional semiconductor materials were found to become soft in nanomembrane or even thin film form.[2,47,129,143] For instance, 100 nm thick Si nanomembranes experience peak strains of only 0.0005% upon bending to a curvature with radius of 1 cm. The strain of this nanomembrane mounted on a plastic sheet with a thickness of 20 mm at similar bend radii was detected to be ~0.1%, which is still below the fracture limit of Si (~1%).[135,137,144] It is worth noting that the strain can be further decreased by moving the Si nanomembrane into the interior of the plastic sheet.[133,144] By thinning the materials into film/nanomembranes, devices on plastic substrates for applications in electronics and photonics have been fabricated.[145–147] Actually, stretchability is a more versatile property compared with bendability, and stretchable electronic or optoelectronic systems should be able to absorb large amounts of strain without fracture or significant deterioration of properties.[137,148–152] In this case, thinning may not be enough. As a supplementary means, the super stretchability is experimentally accomplished by combination of thin films/nanomembranes with pre-defined three-dimensional geometries., e.g. wrinkled or buckled geometries (wrinkled nanomembranes by self-assembly will be discussed in detail in section 4) with a physics similar to an accordion bellows,[153–156] which can further decrease the strain e.g. to 10-20% in Si nanomembranes.[135,157] By applying these considerations, an amazing hemispherical electronic eye camera, which is a digital camera based on an array of single-crystalline silicon photodetectors in the approximate size and curved layout of the human retina, has recently been fabricated and reported,[158,159] and photographs of the device are exhibited in **Figure 6**.[158] Compared to planar systems, curved layouts achieve an improved field of view, increase illumination uniformity and lower aberrations.[135,158] However, we should stress that current flexible and stretchable electronics and optoelectronics are fabricated mostly on thin films with a thickness slightly larger than that of other nanomembranes. Even so, the related research has attracted great interest from nanomembrane researchers due to the similarity in materials and experimental approaches. Stretchable electronics may also be developed into real nanomembrane-based structures with further decreases in thickness in order to reduce strain in the systems.

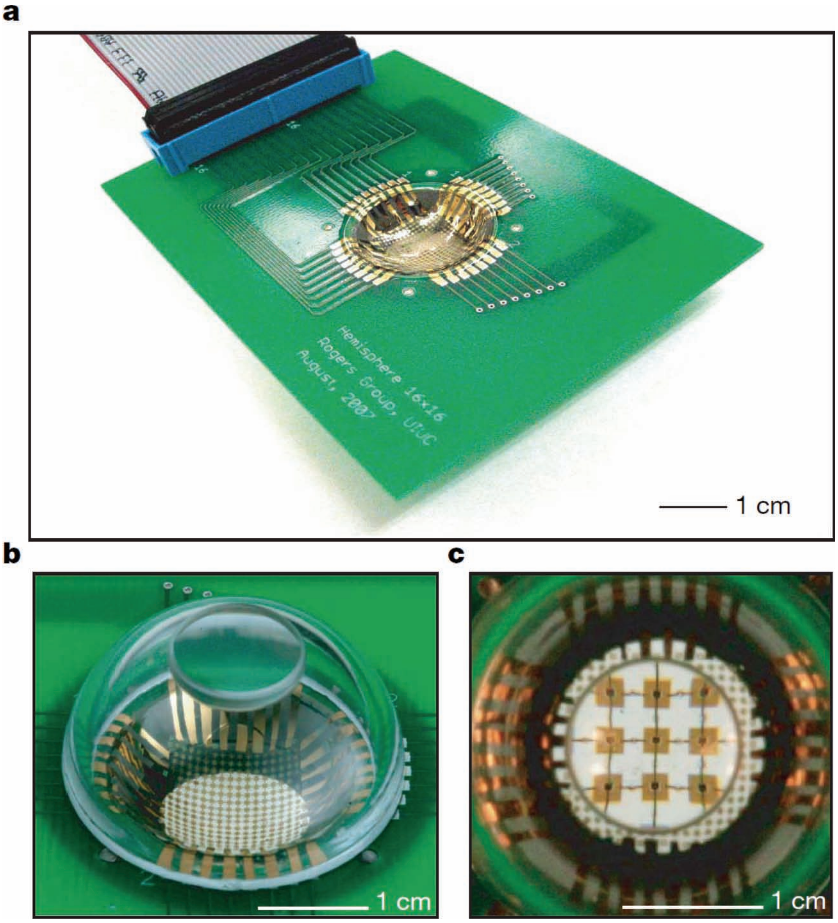

Figure 6. Photographs of a hemispherical electronic eye camera. (a) Photograph of a hemispherical focal plane array mounted on a printed circuit board. (b) Photograph of the camera after integration with a transparent hemispherical cap with a simple, single-component imaging lens. (c) Close-up photograph of the system in (b), taken directly through the imaging lens. Reproduced with permission from ref. [158].

3.2. Magnetic Stretchable Nanomembranes

It is widely accepted that tensile or compressive strain can influence the magnetic and transport properties of a magnetic thin film or nanomembrane in an observable way.[160,161] The generation of the strain in previous research has always been from the lattice mismatch between the thin films/nanomembranes and the substrates, and thus could not be varied in one sample. The development of magnetic stretchable nanomembranes here, on the other hand, provides a straightforward alternative method for investigating the dependence of magnetic properties on strain in nanomembranes where the strain can be changed continuously by stretching.

Investigation of single-layer magnetic nanomembranes shows that the magnetic hysteresis loop, coercivity, magnetic domain structure, and magnetoresistance are all altered due to the magnetoelastic effect.[162] Experimentally, 100 nm Cr nanomembranes have been deposited on plastic substrates by sputtering, and then deformed with various plastic strains.[162] The magnetic anisotropy along the transverse direction increases with strain along the longitudinal axis and is ascribed to the negative magnetostriction.[162] The anisotropic phenomenon was also observed in magnetic domains: their density increases when the magnetic field is aligned along the hard axis while their size increases when the magnetic field is aligned along the easy axis, accompanied by an increase in magnetoresistance.[162]

The influence of strain on magnetoresistance stimulates the investigation regarding its influence on giant magnetoresistance (GMR) effect in multi-layer magnetic nanomembranes. GMR effect has been broadly used in read heads in hard disk drives and nonvolatile memory devices since its discovery in 1988.[163–165] However, the application on stretchable substrates has not been so successful due to a small GMR effect mainly from rough interfacing.[166,167] This drawback has recently been solved by introducing a photoresist layer as a buffer (see **Figure 7**a). With this buffer layer, $(Co/Cu)_{20}$ multi-layer nanomembranes deposited on a polyester substrate show excellent bendability (Figure 7b) and enhanced GMR effect (Figure 7c) simultaneously. The introduction of a photoresist buffer layer improves the interface quality and increases the antiferromagnetic coupling fraction in Co/Cu multi-layer nanomembranes, leading to a remarkable increase in the GMR effect.[168] Bending experiments have confirmed the excellent flexibility and stability of multi-layer magnetic nanomembranes with excellent GMR properties. For the $(Co/Cu)_N$ multi-layer structure, the GMR value can be strongly changed by varying the Cu spacer thickness and reaches its maximum at the first antiferromagnetic coupling maximum ($t_{Cu} = t_{AFM}$) due to the Ruderman-Kittel-Kasuya-Yosida oscillatory feature of the exchange coupling strength,[169,170] which can be easily tuned in stretchable nanomembranes. As demonstrated in the inset of Figures 7d and 7e, an applied uniaxial tensile stress leads to a remnant strain (ε) along the longitudinal direction and a change in t_{Cu}.[168] The corresponding variation in GMR value was experimentally observed and is shown in Figures 7d, 7e, and 7f. If the initial Cu thickness is greater than t_{AFM}, the GMR of a Co/Cu multi-layer nanomembrane rises with increasing strain (Figure 7d). In contrast, if the initial Cu thickness is thinner than t_{AFM}, increasing strain leads to a decrease of the antiferromagnetic coupling strength resulting in a smaller GMR (Figure 7f). If the initial Cu thickness is a little thicker than but very close to t_{AFM}, increasing strain leads to an initial increase and then ultimately a decrease in the GMR value (Figure 7e). The experimental results in Figure 7 clearly demonstrate that that the GMR effect can be mechanically tuned and explained by varying the Cu thickness by applying an external stress to a stretchable nanomembrane.[168] As a step towards a new generation of flexible magnetoelectronic devices, a GMR multi-layer nanomembrane was recently fabricated on an elastic rubber substrate.[171] Thermally induced wrinkles in the nanomembrane allow for high stretchability, with conductivity persisting up to a tensile strain of 4.5%, and due to the elasticity of the substrate, the mechanical deformations imposed on the nanomembrane are totally reversible. Sensing applications involving this type of nanomembrane have been demonstrated at a preliminary stage[171,172] and the cheap and convenient fabrication technique should have significant potentials in future stretchable magnetoelectronics.

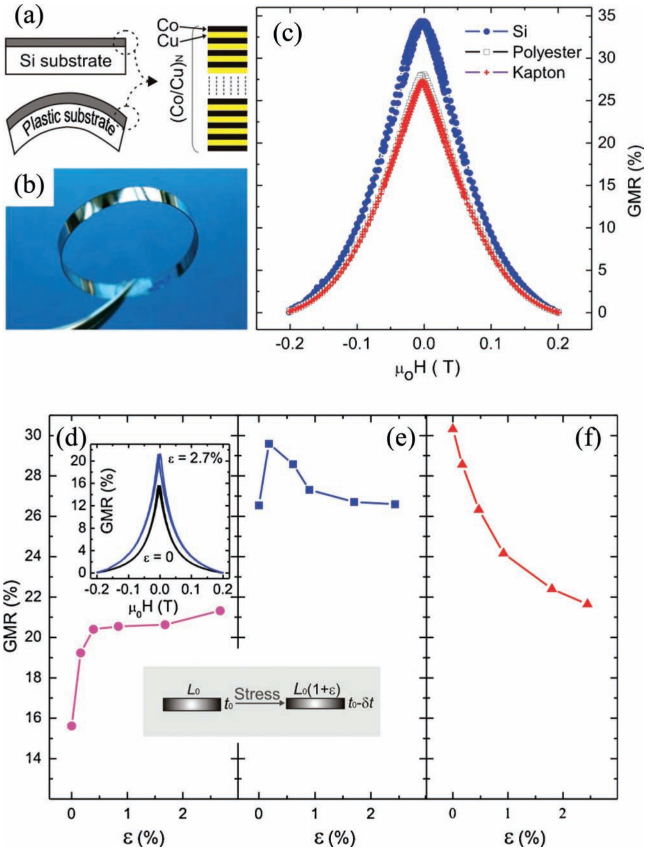

Figure 7. (a) Schematic illustration of a $(Co/Cu)_N$ multi-layer nanomembrane deposited on Si and flexible substrates. b) A photographic image of a circularly bended $(Co/Cu)_{20}$ multi-layer nanomembrane deposited on polyester substrate. c) GMR curves of $(Co/Cu)_{20}$ multi-layer nanomembranes deposited on polyester, kapton, and thermally oxidized Si substrates. (d)–(f) Strain-dependent GMR of $(Co\_1\ nm/Cu\_t\ nm)_{30}$ multi-layer nanomembranes deposited on polyester substrates under 0.2 Tesla with various initial Cu spacer thicknesses of t_{Cu} = 1.027 nm (d), t_{Cu} = 1.014 nm (e), and t_{Cu} = 0.986 nm (f). The top inset in (d) shows the GMR curves before and after strain. The bottom inset in (d) and (e) schematically shows the Cu thickness decreasing under an external tensile strain. Adapted from ref. [168].

3.3. Deformable Graphenes

Graphene is a zero-gap semiconductor with a conical band structure, and its conduction and valence bands are connected at the Dirac point.[173] Therefore, a special issue, creating an energy gap at K and K' points in the Brillouin zone, must be solved before its application in the electronics industry can move forward,[174,175] because a material with a large band gap is indispensable in the fabrication of MOSFET.[175] Several experimental attempts such as graphene nanoribbons or quantum dots fabrication,[176,177] applying perpendicular electric fields to bi-layer graphene,[178] and the chemical modification of graphene,[179] have been carried out to explore the possibility of bandgap opening. The experiments have been partially successful but the defects and lattice imperfections introduce additional localized electron states into the band gap. This leads to so-called variable-range-hopping conduction in the band gap, and correspondingly causes observable leakage current.[175,180] In the case of carbon nanotubes, strain was found to be able to change the energy band structure and open a band gap.[181] Due to their similar structural properties, the opening was also anticipated in graphene. Recently, calculations predicted that a strain along three main crystallographic directions would induce strong gauge fields that effectively act as a uniform magnetic field. This periodic pseudo-magnetic field would correspondingly lead to a Landau-level-like energy spectrum with multiple energy gaps at high energies.[182] So far, most works dealing with the mechanical properties of graphene and its strain are of a theoretical nature due to difficulties in experimentation such as obtaining giant high quality single-layer graphene, and significant discrepancy exists in the simulations.[183–185]

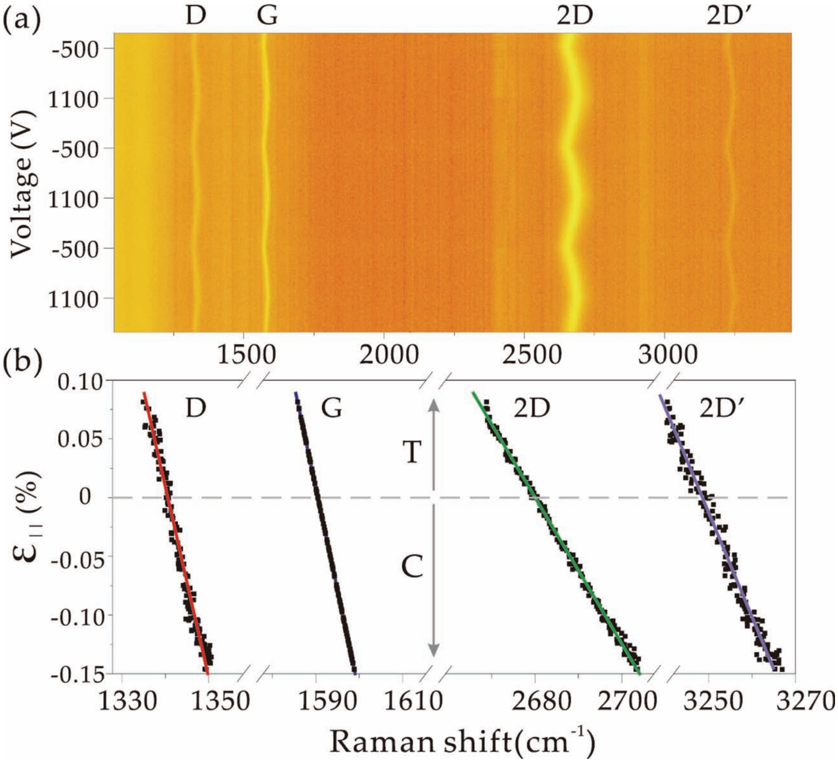

Figure 8. (a) Color-coded intensity map of the Raman peaks as a function of the voltage applied to the piezoelectric actuator. The spectra are fully reproducible over multiple compressing/stretching cycles. (b) D, G, and 2D peaks plotted as a function of the biaxial strain $\varepsilon_{//}$, the solid lines are line fits. T and C represent tensile and compressive strain respectively. Reproduced with permission from ref. [189]. Copyright 2010 American Chemical Society.

In general, the strain can be imposed experimentally by simply stretching or bending the graphene on a flexible plastic substrate,[174,186] and probed optically by measuring the shifts of phonon frequencies. The corresponding Grüneisen parameter has been successfully extracted from the experiments, which is an important fundamental parameter describing the rate of phonon mode softening (or hardening) under tensile (or compressive) strain, and determines the thermo-mechanical properties.[187,188] Nevertheless, uniaxial strain was found to move the relative positions of the Dirac cones and significantly influence the inter-valley double-resonance processes (D and 2D peaks). Thus, biaxial strain, which avoids such perturbations and mimics the experimental conditions where the graphene is supported by a planar substrate, would be more versatile for study concerning strain effects on the double-resonance processes.[189] In a recent report, tunable tensile and compressive biaxial stresses were applied to single layer graphene by utilizing a piezoelectric actuator.[189] The Raman measurement was carried out using a $\lambda_{ex} = 532$ nm laser as an excitation source, and the obtained Raman spectra of the strained graphene are shown in **Figure 8**. For $V>0$, the graphene experiences an in-plane tension (*T*) and the peaks show linear shifts to lower frequencies, while for $V<0$, in-plane compression (*C*) in graphene is realized and peaks correspondingly shift to higher frequencies. Figure 8a also demonstrates that the spectra are fully reproducible over multiple compressing/stretching cycles.[189] The strain-dependent shifts of D, 2D, and 2D' peaks after the strain calculation are plotted in Figure 8b. A linear shift with the biaxial strain is observed, indicating that neither slippage nor corrugation of the graphene occurs during the experiment. The corresponding Grüneisen parameter can be determined to be $\gamma_D = 2.30$, $\gamma_{2D} = 2.98$, and $\gamma_{2D'} = 1.73$, which suggest a strain dependence similar to graphite.[189,190] The different strain sensitivity of the D and 2D peaks is ascribed to the existence of two sub-peaks which compose the D peak.[189] It is worth noting that different Grüneisen parameters are reported by research groups, and several reasons have been considered to cause the deviation: (1) the strength of the strain; (2) the Poisson's ratio of the substrate; (3) intrinsic strain in the graphene layer.[188]

Deforming graphene can lead to formation of other carbon-related structures. For instance, adsorption of atoms onto the surface introduces stress to drive the folding process of graphene, which ultimately leads to fabrication of a single-wall carbon nanotube.[191–193] Microwave irradiation may also cause graphene to be deformed into other morphologies. Researchers found that carbon nanoscrolls exfoliated from graphite could be fabricated with the assistance of microwave sparks in liquid nitrogen,[194] while graphene oxide annealed in solution by microwave sparks leads to formation of graphene nanospheres.[195] In addition, large stretch deformation of graphene beyond its fracture limit leads to the formation of monatomic carbon chains,[193,196] although graphene is a very strong material. The graphene-based nanostructures may also have important applications in MEMS/NEMS.

4. Wrinkled Nanomembranes

If the nanomembrane is forced to extend while the geometrical boundary conditions limit its planar space, it will be wrinkled or buckled in the perpendicular direction. Experimental and theoretical investigations about formation mechanisms of wrinkles have been intensively carried out in the past, and the deformation was found to be described by a set of non-linear partial differential equations (e.g. Föppl-von Karman equation).[197,198] With the rapid development of nanostructures and nanodevices, wrinkled nanomembranes are being pursued for many applications. For instance, nanomembrane wrinkles can help to increase the stretchability in stretchable electronics,[136] as we discussed in section 3.1. Other novel applications in fluidics, mechanical metrology, and strain engineering have also been explored recently.[199]

4.1. Formation of Wrinkled Nanomembranes

Conventionally, wrinkled nanomembranes could be formed by depositing nanomembranes onto an expanded flexible substrate and subsequently restoring the substrate to its original state. The process introduces compressive stress in the nanomembrane, which is then relieved by wrinkling or buckling.[198,200,201] The nanomembranes used in previous research were mainly metal and polymer nanomembranes and the winkles formed show perfect sinusoidal topography.[200,202–204] In fact, wrinkles can form even without external nanomembrane deposition and simply by surface treatment of the flexible substrate. For instance, oxygen plasma treatment of poly(dimethyl) siloxane (PDMS) substrate introduces a layer of silica-like nanomembrane with a thickness of several nanometers, which forms a wrinkled structure upon substrate shrinkage by e.g. cooling.[205–208]

4.1.1. Deterministic Wrinkles in Semiconductor Nanomembranes

The technique was recently expanded by releasing pre-strained semiconductor nanomembranes from underneath a sacrificial layer, and the strain therein is determined by the lattice mismatch between the nanomembrane and the sacrificial layer.[209] Here, we focus on two groups of commonly used material systems: (1) SiGe-on-insulator (SiO_2), where the SiGe nanomembrane is wrinkled after removal of the SiO_2 sacrificial layer; and (2) InGaAs and AlAs, where the InGaAs nanomembrane is grown on an AlAs sacrificial layer. SiO_2 and AlAs can be selectively etched away by HF in even very dilute concentrations.[22,209,210] It is believed that a lower strain gradient with high average strain and longer etching depth leads to wrinkling of the nanomembrane,[211] as demonstrated in **Figure 9**a. The relaxation of the nanomembrane by wrinkle formation lowers the total elastic strain energy in the deformed structure, and this can be reflected in the Raman spectra.[209] It is worth noting that the geometry of the wrinkled nanomembrane is slightly different from that obtained using the conventional method, where a sinusoidal shaped structure was always observed.[201] The morphology variation was observed in the drying process after chemical etching in liquid etchant,[199,209] and was ascribed to the bond-back effect of wrinkled nanomembranes during drying, which is driven by the liquid surface tension. This bond-back effect also leads to interesting micro-/nanochannels formation, as displayed in Figure 9a.

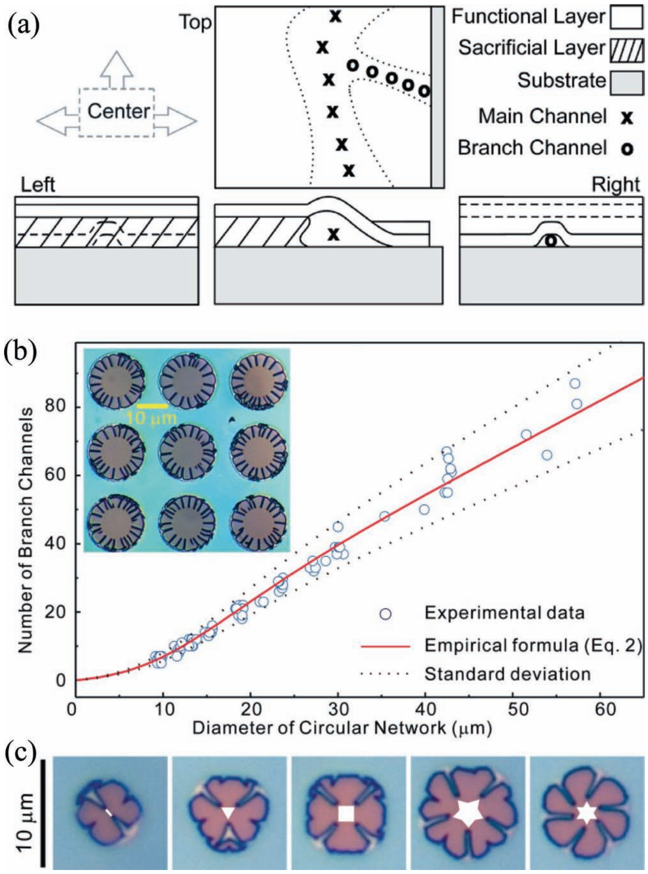

Figure 9. (a) Generic description of the wrinkled nanomembrane and the channels formed. A single unit of such a network consists of a main channel and a perpendicularly oriented branch channel. (b) and (c) Size and shape effects on circular nanochannel networks. (b) The number of branch channels versus diameter of circular network. The inset shows an array of circular networks. (c) Optical images of circular networks with 2-6 well-positioned branch channels. Defined pattern shapes form left to right: short line, triangle, square, and five- and six-pointed stars. Adapted from ref. [209].

Besides the strain status and the thickness of the nanomembranes, the final geometries of the wrinkled nanomembrane are also influenced by the thickness of the sacrificial layer. The effect of sacrificial layer thickness was previously investigated in the InGaAs/AlAs system, where interesting morphology evolution was demonstrated. When decreasing the AlAs sacrificial layer thickness to 40 nm, the channels from the wrinkled nanomembrane assume a two sub-channel Y-like shape with reduced size, reaching from the etching front to the start edge. In the case of a 20 nm thick AlAs sacrificial layer, channels transform into zigzag shapes. If the thickness of the sacrificial layer is ultimately reduced to 10 nm, the channels preserve the zigzag shape but become even smaller.[199] The interaction between the wrinkled nanomembrane and the substrate in the bond-back effect is considered to be the cause of such morphology transformations. For a thin sacrificial layer, wrinkles can easily interact with the underneath substrate surface during the drying process and hence the wrinkled channels become smaller than those from nanomembranes on thicker sacrificial layers.

In the beginning, the wrinkled nanomembrane was investigated with a straight etching front, and the branch channels perpendicular to the etching front were parallel to each other. In fact, the geometry can be even more complicated than this. By defining the start window for chemical under etching, different well-defined branch channel networks can be formed on the basis of a deterministic wrinkling behavior of the pre-strained nanomembrane. For instance, circular wrinkled channel networks can be formed from a circular pattern after etching (see the inset of Figures 9b). Obviously, the length of the branch channels corresponds to the etching time/etching length, while the number of branch channels (M) is determined by the circular perimeter of the predefined structure.[199] The average periodicity of the branch channels (which is calculated from the perimeter of the etching front divided by the number of branch channels) can be described quantitatively on the basis of experimental observation. Here, we consider that the periodicity λ approaches λ_0 when the diameter of the circular etching front (D) tends to infinity and the circular network becomes a linear one. Thus, the periodicity λ of the branch channels can be phenomenologically fitted by the exponential decay function:[209]

$$\lambda = \lambda_0 + C\ \exp(-D/Dc) \tag{1}$$

where C is a constant representing the amplitude of the decay and D_c is the critical diameter. Using the relationship $M\,\lambda = \pi D$ for circular networks, M can be expressed as:[209]

$$M = \pi\, D/(\lambda_0 + A\ \exp(-D/D_c)) \tag{2}$$

A good fitting of Equation (2) to the experimental results is demonstrated in Figure 9b, where the standard deviation of λ_0 from linear networks (17.1%) is introduced into the theoretical fit.[209] These results clearly demonstrate deterministic behavior of the channels' formation in wrinkled nanomembranes with bond-back effect.

Figure 9c shows wrinkled nanomembranes etched from well-defined initial patterns of special shapes (indicated as white shapes in the centre), such as short lines, triangles, squares, and five- and six-pointed stars. In these cases, the formation of the channels is initiated at the corners of each shape, which cannot be observed from a circular etching front. Well-positioned concentric branches are shown in Figure 9c.

4.1.2. Two-dimensional Channel Networks from Wrinkled Nanomembranes

If the pre-strained nanomembranes are released in two dimensions simultaneously, contrary to previous discussion, both the morphology of the wrinkled nanomembrane and the channel networks are different: the entire released nanomembrane will relax randomly and correspondingly form random channel networks. However, if the etching front is defined by specially designed windows of various shapes, the self-assembly of channel networks can be well controlled and even two-dimensionally ordered channel networks have been formed on wrinkled nanomembranes,[210] as shown in **Figure 10**. Obviously, the ordered network is quite useful in integrative micro-/nanofluidics for on-chip applications.

The parameters that influence the morphology of wrinkles in the one-dimensional etching are still applicable but more factors should be taken into consideration. Here, we will discuss the influence of the shape and size of start windows, and also of the distance between them. The configuration space range that was investigated for square and hexagonally patterned networks made of 10 and 20 nm thick InGaAs layers is summarized graphically in Figure 10a.[210] An indicator of the network quality is represented by the size and aspect of the colored circles in the diagram. A given network is considered as "completely ordered" when all windows are connected by one or more direct channels. In a "mostly ordered" network, fewer than one-fourth of channel links are imperfect. For "poorly ordered networks", networks with up to 50% missing or damaged channels are counted. Missing points in the diagram denote completely disordered channels or that the configuration is geometrically forbidden. One can see that square networks exhibit a better quality for large w (side length) and relatively small l (periodicity), while for hexagonal networks, the situation is different: the best ordering was found at intermediate w and large l.[199,210] The optical images of the samples corresponding to the two arrows in Figure 10a are displayed in Figure 10b. Along arrow A, the square networks from 20 nm thick wrinkled nanomembrane with a fixed $l = 5$ μm undergo a transformation from completely random at $w = 1$ μm to mostly ordered at $w = 4$ μm. Thinner InGaAs nanomembranes lead to more complex multi-directional wrinkles/channels (see the left part of Figure 10b). In the hexagonal networks, w is fixed to 2 μm and both 10 and 20 nm nanomembranes exhibit their best ordering for $l = 6$ μm.[210] Formation of both single- and multi-channels is observed in Figure 10b, and the reason is believed to be different in-plane relaxation constraints caused by the configuration of the etching windows.[199,210]

One may note that in section 4.1.1, the wrinkles/channels start from the corners of the pre-defined shape, which can still be observed in square networks. However, no formation of corner-to-corner channels was observed for the hexagonal networks, and this is mainly ascribed to the larger corner angle in the hexagons.[210] The dimensions of the etching window may also have some influence: the channel networks with a small etching window showed that the formation of channels may be favorable at the corners, which is the region with a confluence of strain relaxation in more than one in-plane direction, and with increasing window dimension, channels formed on corners become less important because the strain is relaxed by formation of the channels at the edges.[210]

4.2. Mechanical Properties and Strain Status of Wrinkled Nanomembranes

The strain and mechanical properties of a wrinkled nanomembrane can be determined from the geometry. From buckling theory, it is well known that when a nanomembrane forms a

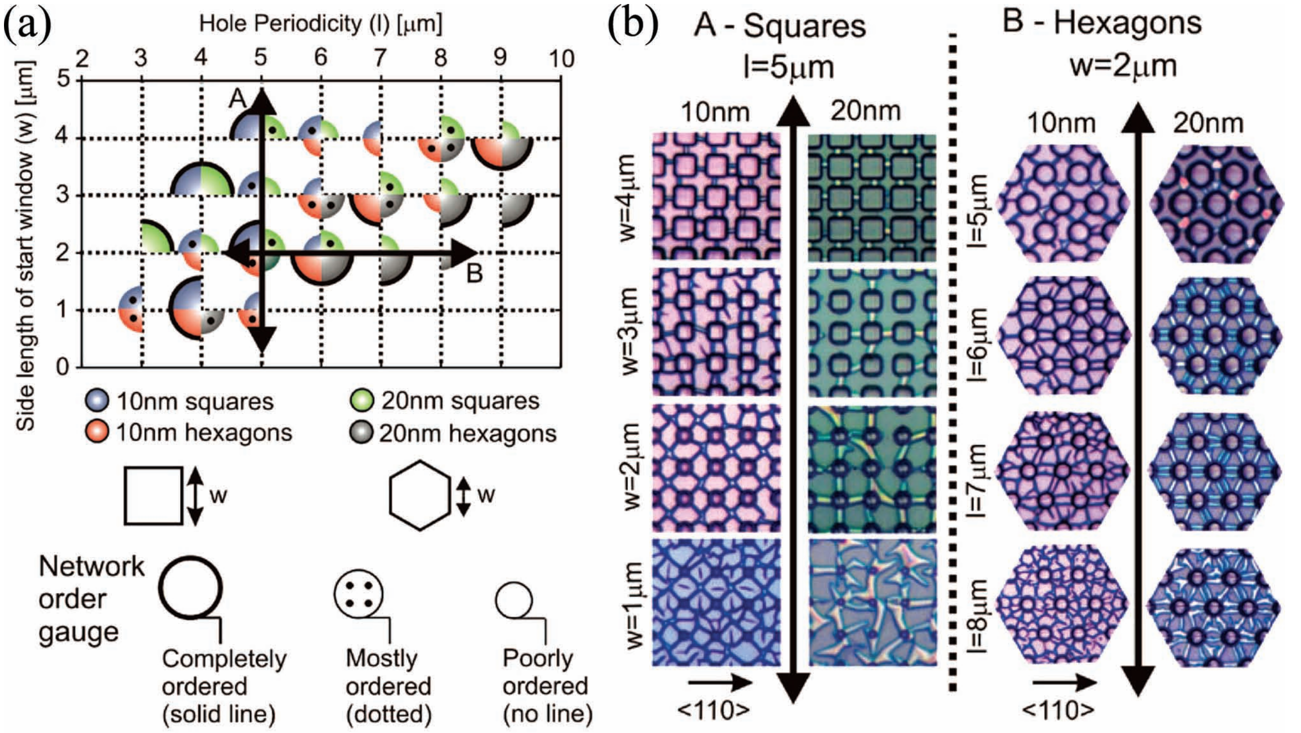

Figure 10. (a) Graphical representation of the configuration space range tested for obtaining square and hexagonally ordered networks from 10 and 20 nm thick InGaAs nanomembranes. A semi-quantitative gauge is used to index the ordering of the obtained network. (b) Optical images of the channel networks for two paths along the arrow A (fixed *l*) and arrow B (fixed *w*). Adapted with permission from ref. [210]. Copyright 2008 American Chemical Society.

stable wrinkle structure, the energy of the system is minimized, and the elastic modulus of the nanomembrane is determined by the periodicity λ.[203,212] Besides direct measurement from microscopy, the λ was previously measured optically in transparent nanomembranes. For instance, the wrinkles can act as a grating to scatter light and the distance between the diffraction spots are inversely proportional to the periodicity λ, which can thus be calculated more accurately.[203,213] The mechanical properties of many polymer and organic nanomembranes have been characterized using this approach.[212,214] The morphology of the wrinkled nanomembrane was also employed to estimate the residual stress in the nanomembrane and cross-link density of the polymer nanomembrane.[204,215]

In fact, the strain and deformation of the wrinkled nanomembranes has also been indirectly investigated using optical methods. For instance, Raman spectroscopy showed a Raman shift of 7 cm^{-1} for SiGe nanomembranes before and after under etching, and a 1.1% compressive strain before etching was calculated.[209,216] Photoluminescence can be used to check the strain status of the wrinkled nanomembrane as well because the strain changes the band structure of the materials. To realize the detection, a luminescent InGaAs quantum well was embedded into a GaAs nanomembrane and acted both as a local strain sensor and strain source, and therefore the shift of quantum well emission indicates the strain state in the layer after deformation.[22,199] The lattice deformations and different strain states in an unetched nanomembrane and in a wrinkled nanomembrane, including the bonded-back and the wrinkled region, are schematically displayed in **Figure 11**a.[22] Before etching, the compressive strain is fully confined in the quantum well (see left panel of Figure 11a). In the bonded back state the layer is released from the substrate and then partially relaxes its internal strain. The tensile stress of the barrier layers (above and below the quantum well layer) is induced by the partial relaxation of the strain in the quantum well layer due to a strain energy minimization (see middle panel of Figure 11a).[217,218] For the wrinkled case in the right panel of Figure 11a, the bending of the nanomembrane produces an inhomogeneous strain distribution where the lattice constant along the growth direction depends on the inner lattice constant and the curvature varies with the distance from the inner wrinkle surface to the outer surface.[22,218] Assuming a position for the neutral plane (dotted line),[219] we can obtain the residual forces, which can be tensile or compressive as shown in the right panel of Figure 11a. Based on the strain status and linear deformation potential theory,[220] the band diagram of the quantum well can be obtained and is shown in Figure 11b.[22] In order to gain an insight into the strain status of the nanomembrane, the calculated transition energies as a function of curvature are given in Figure 11c for three different models. The first model assumes strain energy minimization at a predefined curvature (Bent QW I), while in the second model, the neutral plane is assumed to sit at the center of the quantum well (Bent QW II). A variable position of the neutral plane as a fitting parameter is considered in the third model (Bent QW III). The transition energies from experiments for the strained and partially relaxed

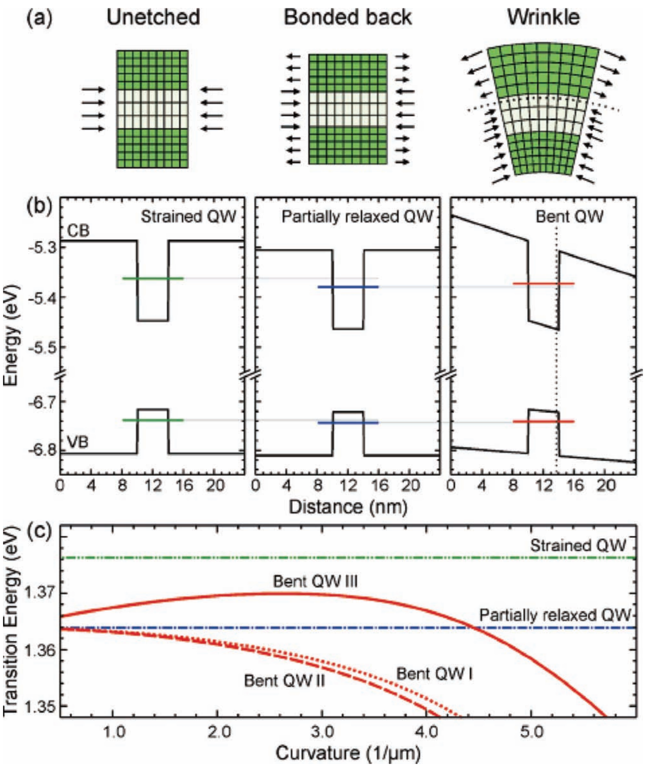

Figure 11. (a) Lattice deformation of unetched, bonded back, and wrinkle structures. Arrows represent the force applied to the layer, and the dotted line in the wrinkle structure indicates the neutral plane. (b) Band diagram corresponding to the structure shown in (a). The lines in the middle of the quantum well represent the quantized energy levels of the electrons in conduction band (CB) and heavy holes in the valence band (VB). (c) Transition energy of the bent quantum well as a function of the bending curvature. Three models are presented. The transition energies from experiments for the strained and partially relaxed quantum well are also plotted as horizontal dashed-dotted lines. Reproduced with permission from ref. [22]. Copyright 2007 American Chemical Society.

quantum well are also plotted as horizontal dashed-dotted lines in Figure 11c for reference. Obviously, the experimental results are inconsistent with the first and the second model, indicating that the wrinkle experiences a complicated strain state, which is probably caused by external forces originating from the bond-back effect during the drying process.[22,199]

4.3. Applications of Wrinkled Nanomembranes

Most applications of wrinkled nanomembranes are related to micro-/nanofluidics. For the wrinkled nanomembranes formed on a flexible substrate, the geometry of the wrinkles can be tuned. The dynamic modulation of the wrinkle has been used to actively manipulate fluidic transport in the wrinkle/channel.[221] By engaging in such an approach, control and manipulation of small objects including nanoparticles as well as DNA molecules in the liquid have been realized.[221,222] Fluidic stretching of DNA in such tunable channels provides a new possibility for molecule linearization and could offer a new platform to investigate the dynamics of DNA at the single-molecule level. Similarly, sieves have been developed from wrinkled nanomembranes to select colloids with sizes corresponding to the wrinkle geometry. A separation experiment was carried out using an aqueous suspension comprising particles with diameters of 67 nm, 3 μm, and 10 μm, and wrinkled nanomembranes with periodicity of ~50 nm, ~1 μm, ~5 μm, ~50 μm, and ~0.4 mm. It was shown that 67 nm particles are collected by the 1 μm wrinkles, those of 3 μm prefer to stay with 5 μm wrinkles, and most of the 10 μm particles were collected by the 50 μm wrinkles.[205] These experiments demonstrated the potential capability of wrinkled nanomembranes in curvature-dependent biophysical processes.[206]

A wrinkled surface of sinusoidal topography also provides a geometric confinement for colloid assembly due to the grooves. Liquid flow[205,206] and dip coating[202] can be applied to align the colloids. The deposition geometry of colloids is easily manipulated by using wrinkles with different geometries (periodicity and height). Since the colloid assembly on wrinkles depends much on the resistance of the raised parts of the wrinkles, the alignment phenomenon of the colloids seems more related to the height of the wrinkles.[199]

The nanofluidic transport as well as the femto-liter filling and emptying characteristics of an individual semiconductor wrinkle have been recently demonstrated.[209] As exhibited in Figure 9a, the single branch channels should all be connected with the main channel. The interconnection of branch channels is easily revealed by adding a Rhodamine 6G dye solution locally to one spot on the network. The filling and emptying were thus clearly observed using conventional fluorescence microscopy, and the change in surface energy during channel filling and emptying leads to two different fluid shapes (i.e. arc- and brick-like) which are described by the Young-Laplace relation, and fluid shape transformation at a certain critical volume can thus be explained.[209] The method may be further developed to investigate the properties of various fluids. By using a similar approach, researchers have recently developed a fully integrated nanofluidic device for ion field effect transistors. KCl as a model electrolyte solution was tested for ion separation, paving the way for future applications of wrinkled nanomembranes in bio-analytic systems.[223]

5. Self-rolled Nanomembranes

5.1. From Wrinkling to Rolling

As we demonstrated in the section 4, nanomembranes wrinkle according to predefined strain engineering to form three-dimensional structures with a variety of potential applications. However, wrinkles are not the only three-dimensional structures that can be formed by the architecting of nanomembranes, and a number of three-dimensional micro-/nanostructures have been produced by nanomembrane rolling or bending.[2,224] In general, if the strain gradient is large, the nanomembrane bends into a curved structure, while for a small or zero strain gradient the nanomembrane wrinkles.[211]

Nanomembranes with isotropically elastic properties were investigated in detail to disclose the mechanism which quantitatively determines the wrinkling or bending/rolling.

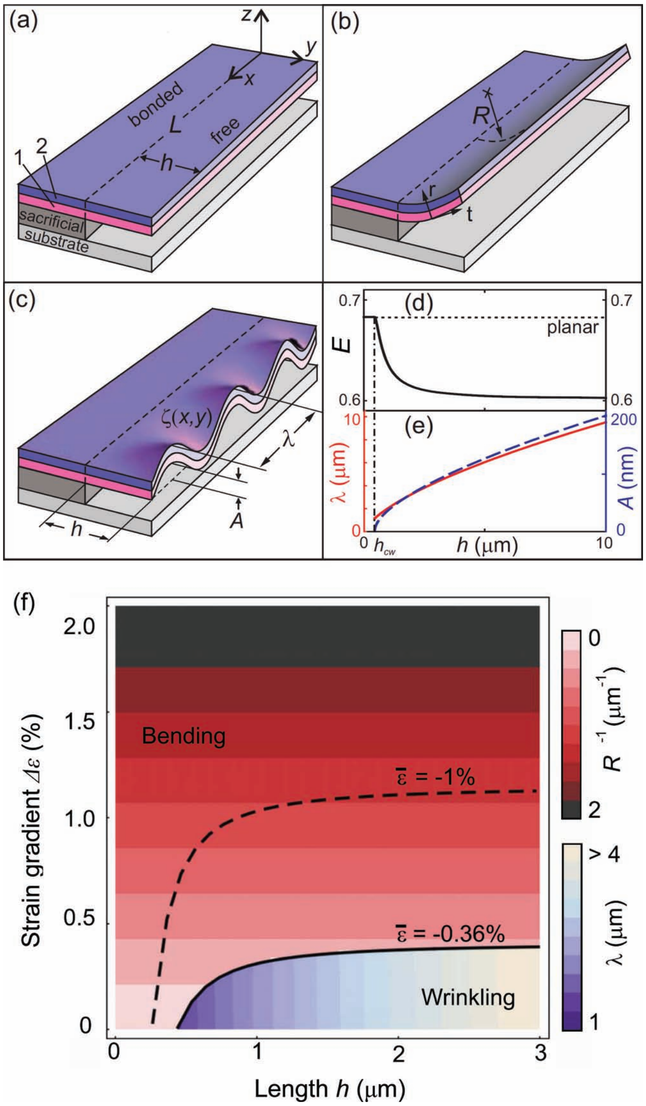

Figure 12. Schematics of (a) a flat bi-layer nanomembrane, (b) a bent nanomembrane with radius *R*, and (c) a wrinkled structure with deflection profile $\zeta(x, y)$, amplitude (height) *A*, and periodicity (wavelength) λ. (d) Wrinkle energy (solid line) and energy of planar relaxation (dashed line) as a function of distance *h*. (e) λ (solid line, left axis) and *A* (dashed line, right axis) as a function of *h*. Vertical dotted-dashed line marks the critical wrinkle length h_{cw}. (f) Phase diagram of favorable shapes based on the energetic comparison between bent and wrinkled structures. The solid curve indicates the boundary between the two. Radius *R* is shown for the bent structure and λ for the wrinkled structure. The dashed curve shows the phase boundary curve for $\bar{\varepsilon} = -1.0\%$. Adapted with permission from ref. [211]. Copyright 2009 American Physical Society.

The three-dimensional structures of a partially released bi-layer strained nanomembrane are schematically shown in **Figure 12**.[211] The bi-layers with thicknesses d_1 and d_2 are subjected to biaxial strain ε_1 and ε_2 respectively. The nanomembrane is free hanging over a distance *h* and is initially in an unrelaxed strained state over the whole length *L*. The released portion is free to elastically relax, constrained only by the fixed boundary (see the dashed line in Figure 12a) where the film attaches to the substrate.[211] The average strain and strain gradient of the bi-layer are defined as $\bar{\varepsilon} = (\varepsilon_1 d_1 + \varepsilon_2 d_2)/(d_1 + d_2)$ and $\Delta\varepsilon = \varepsilon_1 - \varepsilon_2$ respectively. When *h* is small, the fixed boundary (dashed line) confinement in the x direction limits relaxation in x and the strain is relaxed via bending in the y direction (Figure 12b). With increasing *h*, the constraint from the fixed boundary weakens, and strain can now be relaxed via bending and stretching in both directions.[21] However, there is still a geometric constraint for strain relaxation in the x direction, thus stretching/bending with a constraint leads to formation of wrinkles (Figure 12c), and the real shape might be a combination of bent and wrinkled structures.[21,211,225,226] Obviously, there is a minimum *h*, defined as critical wrinkle length h_{cw}, for wrinkle formation. The value of h_{cw} is theoretically found to be $h_{cw} \approx 2.57 d_2 \sqrt{-\bar{\varepsilon}}$.[211] The wrinkle energy as a function of *h* is displayed in Figure 12d, and for $h<h_{cw}$, only planar relaxation in the y direction is obtained (dashed line in Figure 12d). For $h>h_{cw}$, wrinkling can occur and both periodicity λ and height *A* increase with *h*, as demonstrated in Figure 12e. However, $h>h_{cw}$ doesn't guarantee the formation of wrinkles. It is experimentally found that large *h* also allows the bi-layer to roll if the strain gradient (or $\Delta\varepsilon$) is large. A wrinkled structure only forms when the strain gradient is small enough even if *h* is larger than h_{cw}.[21] The preferable shape of the nanomembrane after release is determined by comparing the energies of the bent and wrinkled shapes,[211] which are functions of strain gradient, etching length, and layer thickness.[21] For a typical bi-layer nanomembrane consisting of 10 nm $In_{0.1}Ga_{0.9}As$ and 10 nm GaAs, Young's modulus $Y = 80$ GPa and Poisson ratio $\upsilon = 0.31$, the ε_1 and ε_2 were systematically changed to calculate the favorable shape as a function of *h* and $\Delta\varepsilon$, and the obtained phase diagram is shown in Figure 12f. One can see that when $\Delta\varepsilon = 0.20\%$ and $\bar{\varepsilon} = -0.36\%$, bending will be favored only until *h* is increased to 700 nm. With further increasing *h*, the wrinkled structure requires a lower energy than the bent structure and thus becomes favorable.[211] For higher $\bar{\varepsilon}$, the phase boundary curve moves upwards (see dashed line in Figure 12f) and the wrinkling region is enlarged.[211] Figure 12f also indicates that in the wrinkling region, the λ increases with increasing *h*, while in the bending region, the radius of the bend structure decreases with increasing $\Delta\varepsilon$.

If the nanomembrane has anisotropically elastic properties, the situation is slightly easier. To simplify the description, the coordinate system is defined as the same as that in Figure 12a. If the y direction is the most compliant direction, the nanomembrane will bend or roll in this direction.[21] Conversely, if the x direction is the most compliant direction, the critical length h_{cw} should also be taken into consideration. When $h<h_{cw}$, the fixed boundary (dashed line in Figure 12a) does not allow the strain to relax along the x direction, and the strain will be retained. When $h>h_{cw}$, the nanomembrane attempts to bend/roll in the x direction, and the constraint thus causes the formation of wrinkles.[21] This behavior has been demonstrated experimentally, where λ decreases while *A* increases with increasing *h*.[227]

5.2. Tube or Spring?

As we know, three-dimensional structures may be architected by the bending, rolling, or curling of nanomembranes.[29,224,228]

These three-dimensional architectures can be sophisticatedly designed by shaping the nanomembrane prior to bending/rolling using, for example, photolithography, as we have discussed in section 1.3. The anisotropy in the strain/stress also remarkably influences the geometries of the structures because the nanomembranes prefer to bend/roll along the compliant direction due to the elastic energy minimization. For instance, the <100> directions in single crystal Si are the most compliant with the smallest Young's modulus, and the rolling along this direction is energetically favorable.[47,229] Therefore, if the nanomembrane is released (for example, by chemical under etching) along the most compliant direction, micro-/nanotubes will be formed.[26] If the nanomembrane is pre-shaped into a strip, rolling along the most compliant direction will cause the formation of micro-/nanoring.[21,230] However, if the orientation of the strip is misaligned with the most compliant direction, the rolling along this direction thus leads to formation of helical structure, as reported in InGaAs/GaAs, SiGe/Si, and SiGe/Si/Cr systems.[231–233] In all cases, the anisotropy in the stiffness leads to rolling along the <100> directions, and thus the geometries of the obtained helical structures are mainly determined by the nanomembrane thickness and the misaligned angle between the strip orientation and <100> directions.[231–234] Moreover, experimental observation indicates that the angle between the strip and the closest <100> direction decides the resulting helical structures, and the phenomenon is considered to be due to the significant influence of the etching behavior since the etching is also anisotropic.[232] In samples with SiGe/Si or SiGe/Si/Cr nanomembranes on a single-crystal Si substrate (also serving as the sacrificial layer), the smaller the angle between the strip and the <100> directions, the faster the etching speed. For strips aligned closer to the <110> direction, the (111) facet rapidly forms at the sides of the strip during the under etching, which is the plane with the lowest etching rate, hampering etching from the sides, and the etching approaches predominantly from the front end of the strip. A further increase in the misaligned angle between the orientation of the strip and the <110> direction leads to an increase of under-etching from the sides, causing a faster release of the strip.[231,235] Consequently, for a strip misaligned with the <110> direction, its angles with respect to the neighboring two <100> directions are different, and the etching rate from the two sides of the strip are also different. The larger angle (>45°) determines which side of the mesa is fast etched, and therefore the strip scrolls along the (100) direction with a larger angle, causing different chiralities in the obtained springs.[232] According to this anisotropic etching behavior, one may infer that the helicity angles of the obtained helical structures are always larger than 45°, and their applications could be limited. This restriction was found to be overridden in so-called anomalous coiling with very narrow strips.[233] In this case, the edge effect causes strain relaxation at the sides of the strips, leading to an asymmetrical lattice distortion and, in turn, to a uniaxial strain component along the strip. This effect dominates the rolling in narrow strips and thus helical structures with helicity angles less than 45° have been obtained.[233,236] Similarly, an additional Cr layer which is isotropically tensile stressed may also partially override the anisotropic Young's modulus of semiconductor nanomembranes, resulting in anomalous coiling. The deviation increases with decreasing strip width and increasing Cr layer thickness.[233]

The nanomembranes with isotropic strain gradients were, on the contrary, predicted to be rolled into tubular structures by the classical Timoshenko formula.[2,237] Obviously, since the nanomembrane is elastically isotropic, the nanomembrane should be rolled along all directions.[21] Minimization of the bending energy makes the nanomembrane roll/bend with an optimal radius independent of the rolling direction, as always observed experimentally.[21] However, if the rolling length of the nanomembrane (or the strip with width W cut from the nanomembrane) is longer than the perimeter length L_0 of the tube, more rotations will be formed with increasing radius. Theoretically, in the case of narrow strips, the strain gradient may lead to the formation of a helical structure by choosing a rolling direction with an angle θ to the long side of the strip, with all the rotations in the helical structure adopting the optimal radius. In such structures, the bending energy is minimized but with some cost in shear energy, but the total energy must always be smaller than in the tube case where additional bending energy is produced due to the deviation of the larger radii from the optimal value.[2,21,238] It is worth noting, though, that in real three-dimensional structures from self-rolled nanomembranes, the additional bending energy from increasing radius is almost negligible due to the small thickness of the nanomembrane. There is also a geometrical restriction for helix formation: the rolling angle θ must be larger than a critical value $\theta_c = \sin^{-1}(W/L_0)$. If $\theta<\theta_c$, otherwise neighboring rotations in the strip overlap (helix pitch<0), and thus a tubular structure is obtained.[2,238] A detailed phase diagram for tube-vs-spring formation can be found in ref. [238].

As one can see the formation of both tubes and springs is from bending/rolling of nanomembranes driven by the stress, and therefore, the science and technology therein are quite similar. As for the potential applications, both have attracted increasing interest during the past few years. The helix is a flexible structure which has potential in electromechanical force sensors,[231,239] while tube has capability in an even broader range of applications (as will be discussed in section 5.4).

5.3. Rolled-up Nanotechnology

For the fabrication of rolled-up microstructures like micro-/nanotubes or springs, the introduction of a strain gradient perpendicular to the nanomembrane is a must. It is worth noting that the strain gradient may also cause wrinkling of the nanomembrane in certain circumstances as discussed in section 5.1. Several approaches have been proposed, the first of which is utilizing lattice mismatch in epitaxial bi-/multi-layer nanomembranes. Group IV,[26,29,224,234,238] III-V,[28,34,240,241] and even II-VI[242] semiconductor materials have been successfully strain-engineered and rolled. The biggest advantage of this method is the controllability: on the basis of the well-known values of the lattice constants, researchers can calculate the strain accurately, which is of benefit to the experiments' design.[228,234] For instance, a Ge layer epitaxially grown onto a Si(001) substrate creates a 4% misfit strain at the interface if the Ge is fully strained.[21] In compound semiconductor materials, the lattice constant varies with the composition and thus the strain can be tuned, which improves the scalability of the rolled-up micro-/nanotubes. Nevertheless, in an epitaxial nanomembrane with thickness beyond the critical value, the nanomembrane is no longer coherent and plastically relaxed via dislocations, and thus the previous calculation considering only lattice mismatch is not correct. Beside the expensive epitaxial nanomembranes, nanomembranes deposited by other non-epitaxial vapor deposition may also be inherently strained, containing built-in stress.[21] The strain status normally depends on the experimental parameters during deposition, and can be manipulated to generate the required strain gradient.[230] The third method used to introduce strain and strain gradients into the nanomembranes is to heat or cool the materials system with different coefficients of thermal expansion.[21]

By combining the two latter approaches, researchers have demonstrated a versatile method to roll nanomembranes of a number of inorganic materials and their combinations from a polymer sacrificial layer. As exhibited in **Figure 13**a, a pre-stressed inorganic nanomembrane deposited onto a polymer sacrificial layer (here: photoresist) is released by removing the sacrificial layer with acetone or other organic solvents and rolls-up into a micro-/nanotubular structure.[42] The advantage here is that acetone can etch a photoresist sacrificial layer over almost any inorganic material with practically 100% selectivity. Figures 13b-13i show examples of rolled-up microtubes: b) Pt, c) Pd/Fe/Pd, d) TiO_2, e) ZnO, f) Al_2O_3, g) Si_xN_y, h) Si_xN_y/Ag, and i) diamond-like carbon. Since the photoresist layer can be easily patterned using conventional photolithography, the above nanomembrane is self-patterned during deposition (see also section 1.3). This provides obvious convenience in accurate positioning of microtubes and module integration on a single chip, as preliminarily demonstrated in Figure 13j for a SiO/SiO_2 microtube array.[42] One can see that microtubes of

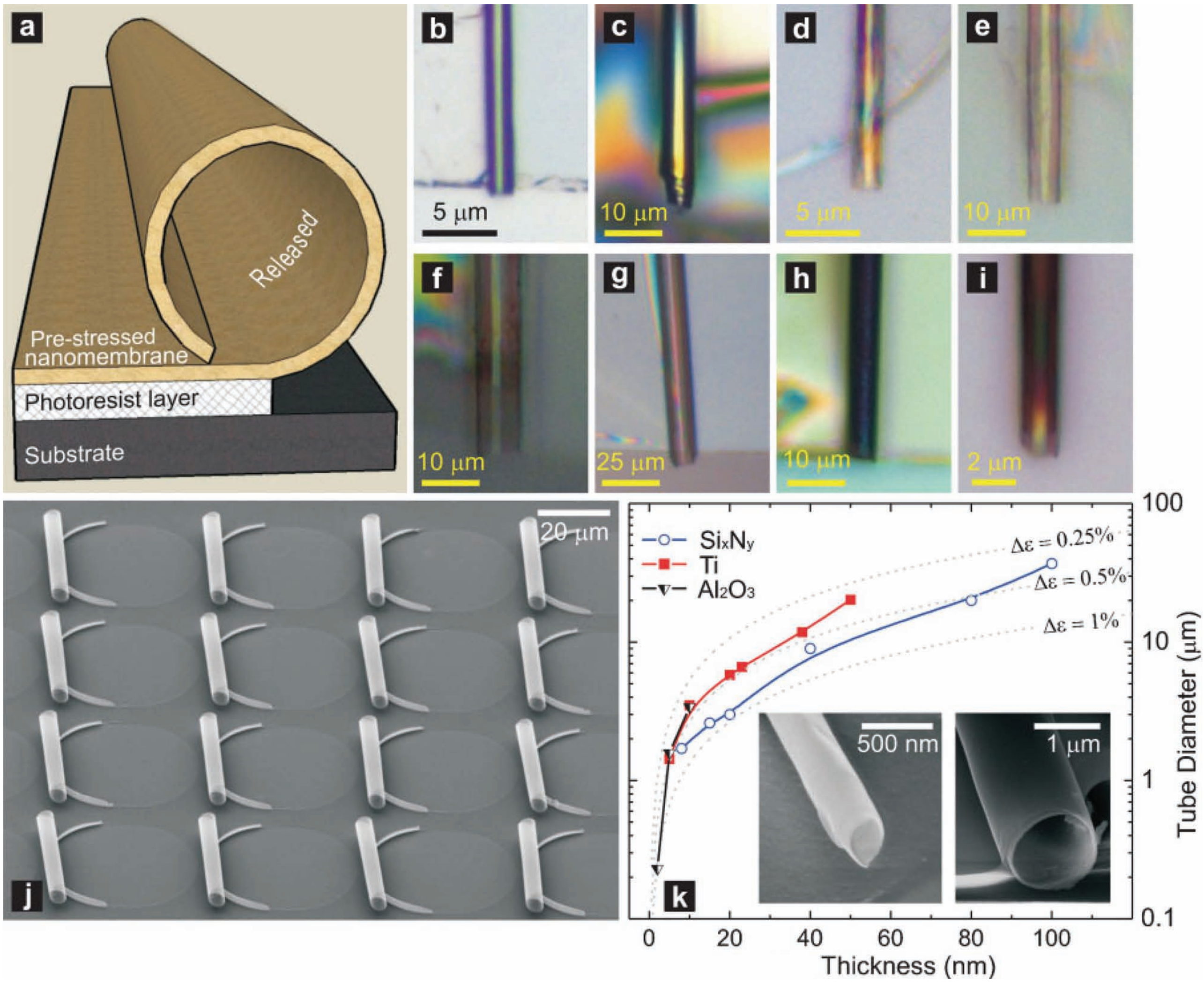

Figure 13. a) Schematic diagram illustrating the rolling process of a nanomembrane on a polymer sacrificial layer; optical images of rolled-up microtubes made out of b) Pt, c) Pd/Fe/Pd, d) TiO_2, e) ZnO, f) Al_2O_3, g) Si_xN_y, h) Si_xN_y/Ag, and i) diamond-like carbon; j) a scanning electron microscopy image of an array of rolled-up SiO/SiO_2 microtubes; k) tube diameters as a function of thickness for various materials: Si_xN_y (blue open circles), Ti (red filled squares), and Al_2O_3 (black half-filled triangles). Left inset shows a scanning electron microscopy image of an Al_2O_3 microtube with a diameter of ~230 nm. Right inset displays a scanning electron microscopy image of a Si_xN_y microtube. Adapted from ref. [42].

well-defined length and geometry and the same orientation have been arranged into a periodic array. The strain gradient in nanomembranes deposited on a photoresist layer originates from both inherent built-in strain and a difference in thermal expansion between the deposited materials and the photoresist layer. Specifically, during nanomembrane deposition two factors need to be considered for microtube formation.[42] Firstly, the evolution of substrate (including photoresist layer) temperature, and secondly the deposition rate and the base pressure during deposition. Alternative deposition rates may also lead to different grain sizes in the nanomembranes, which in turn exert different stress levels.[243] Similar to other rolled-up microtubes, the diameter of microtubes produced by this method can also be well-tuned by changing the thickness and the strain gradient of the nanomembranes, as shown in Figure 13k.[42] However, it is worth mentioning that unlike the epitaxial defect-free nanomembranes, an accurate analytical description of the strain gradient and the microtube diameter in such cases is not possible. In addition, the nanomembranes deposited on photoresist layers are always of poly-crystal or amorphous nature, which may influence their properties for future applications.

Besides the strain gradient from the structural properties of the materials in nanomembranes, it is believed that changes to the surface structure of the nanomembrane, such as surface reconstruction, can create a strain gradient perpendicular to the nanomembrane. Investigation proves that the clean Si (001) surface exhibits a (2×1)-type reconstruction and predicts that in an odd-layer nanomembrane, a surface-stress imbalance exists between its top and bottom surfaces, creating a unique self-driving force to bend the nanomembrane.[244] However, due to the inherent difficulty of the experiment, only theoretical simulation has so far been presented.

Of course not only inorganic materials but also organic materials themselves can be rolled into tubular structures.[245–248] The rolling is induced by different swelling properties of chemically dissimilar polymers in selective solvents, and the forces arise in response to an unequal change in the volume of certain components in the bi-layer polymer nanomembrane.[245] For instance, polystyrene (PS) and poly(*4*-vinylpyridine) (P4VP) can be dip-coated onto a Si substrate to form a bi-layer structure. Upon exposure to water, PS demonstrates minimal water uptake, forming a stiff hydrophobic layer. P4VP is less hydrophobic and swells in acidic aqueous solutions because of the protonation of the polymer chains.[245–247] Polymer combinations with such mechanical effects can also be employed for rolled-up microtubes.[248] A thin layer of other inorganic material may also be incorporated into this kind of polymer microtube to alter the physical properties of the microstructure.[245,246] The use of biocompatible polymers for rolled-up microtubes may pave their way for potential uses in biotechnology.[248]

5.4. Applications of Self-rolled Nanomembranes

So far, rolled nanomembranes and related structures have been made from many different materials and material combinations. These kinds of three-dimensional structures have the ability to combine the excellent properties of the constitutive materials with their unique geometries and thus possess novel features in their mechanical,[31,231] optical,[34,36] electrical,[32] and magnetic[249] properties, which also implies a potential for advantageous applications in various fields. Because of this, the number of related publications is rapidly increasing. In the following sections, we will summarize the most important applications of the self-rolled nanomembranes.

5.4.1. Optical Resonators and Metamaterials

Recently, design and fabrication of novel label-free optical sensors based on ring resonators, which filter and confine light at certain resonant wavelengths in small volumes, have started to attract increasing attention.[250–254] Studies on light emission properties of rolled-up microtubes showed that they can be used as optical resonators,[255–259] and the emission spectra normally show a modulation ascribed to optical resonance (see **Figure 14**a), which originate from light circulating and interfering constructively in the circular cross-section of the microtube.[260,261] In these reports, typical materials used for optical resonators are group III-V semiconductor materials[255,256] and Si-related materials.[34,260] For the first case, the nanomembranes were grown using MBE and thus are of high quality,[255,256] while for the latter case, the nanomembranes can be deposited through epitaxy[34] or evaporation.[42,260] In order to investigate the properties of the resonator, luminescent materials need to be incorporated into the rolled-up microtube, which then emit light under external excitation. Therefore, In III-V microtubes, luminescent quantum dots were embedded during MBE growth.[255,256,258] On the other hand, in Si-related materials, light emission is considered to originate from the luminescent defect centers in SiO_x obtained by thermal oxidation or evaporation.[34,260] As we know, the epitaxial nanomembranes are usually better in terms of the crystal quality and the accurate controllability of the strain gradient, which leads to formation of microtubes with perfect geometry, and thus the quality factor of obtained resonators can reach as high as 3000.[255] The amorphous nature of SiO_x deposited on a polymer sacrificial layer causes strong light loss during light circulation in the tube wall and the observed quality factor is normally less than 1000.[260] However, cheap and convenient fabrication of SiO_x microtubular resonators is still promising and resonators made out of other optical materials may be fabricated in the future via a similar approach.

Since the optical resonance comes from the constructive interference of the light travelling inside the tube wall, one may infer that the geometry of the rolled-up microtube should have significant influence on resonant behavior. Theoretical simulation has indeed proved the sensitivity of resonant wavelength (mode position) to the geometry of the rolled-up microtube: the degenerated modes present in conventional cylindrical cavities are broken and separated into two modes due to the spiral asymmetry of the rolled-up microtubes and corresponding light propagation.[262] Experimentally, microtubes with different geometries have different resonant wavelengths.[34] Even the emission spectra measured along the tube axis show obvious shift, demonstrating the inhomogeneity of the microtube, because for each position of the microtube, the circular waveguide (cross-section perpendicular to the microtube) could be slightly different.[255,259,260] In addition, due to the limited

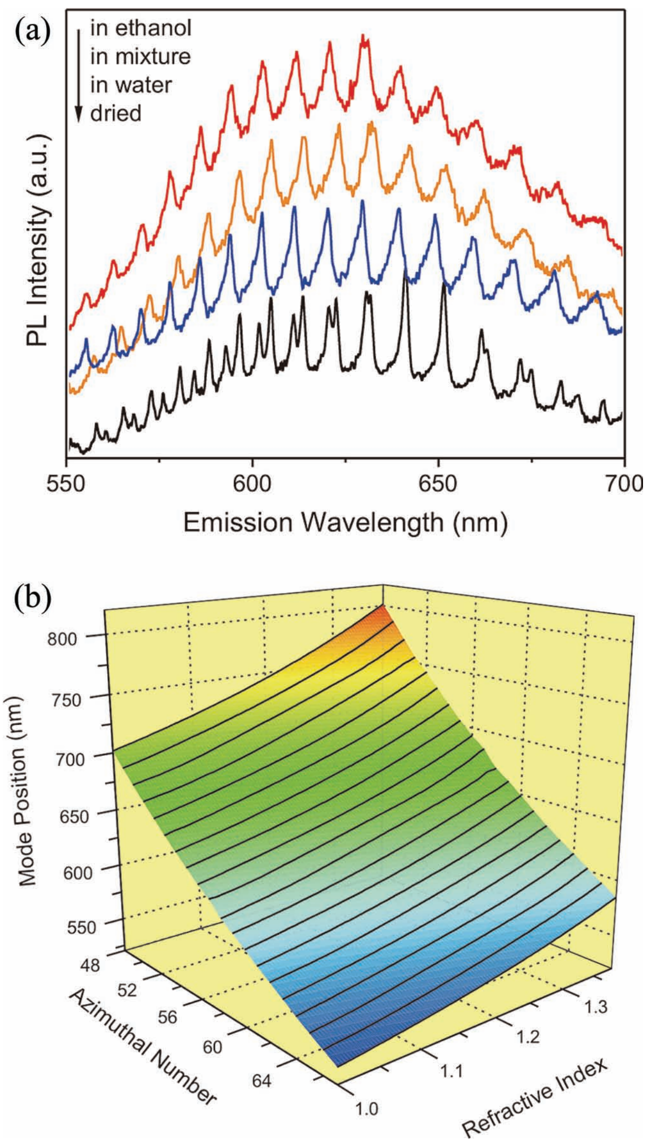

Figure 14. (a) Emission spectra of an optical microtubular cavity with a diameter of ~9 μm in air, de-ionized water, ethanol, and water/ethanol mixture (1:1 in volume). The intensity of each spectrum is normalized to its strongest mode. (b) Calculated modes positions from a rolled-up microtube with a diameter of ~9 μm as a function of azimuthal number and refractive index of surrounding medium. The azimuthal numbers are discontinuous integers indicated by solid lines. Adapted with permission from ref. [261]. Copyright 2010 American Chemical Society.

length of the microtube, light can experience total internal reflection also along the axial direction, which leads to a three dimensional confinement.[258,259] By intentionally designing a rolling edge, researchers have effectively controlled the light confinement in the axial direction.[258] Lobes of parabolic, triangular, and rectangular shapes have been fabricated at the rolling edge, and sharp sub-peaks (eigenmodes) were observed in the experiment.[258] The measured eigenenergies can be described by a straight and intuitive model using an adiabatic separation of the circulating and the axial propagation, where a quasi-potential from actual geometry of the rolling edge needs to be considered.[258]

The unique structure leads to important applications. The luminescent centers are intrinsically located very close to the maximum optical field intensity which raises the quantum efficiency and enhances stimulated emission for lasing, because the excitation light generates carriers only inside the tube wall. The confinement of both carriers and photons may lead to lower lasing thresholds.[255] Experimental results concerning rolled-up microtube lasers were reported recently, and a low threshold of ~4 μW has been achieved.[257,263] Moreover, due to a tube wall that is generally thinner than the light wavelength, the light energy cannot be completely confined within the resonator wall. The evanescent field penetrates into the low refractive index medium around the resonator and interacts with the materials near the interface, accompanied by a wavelength shift of the optical modes.[261,264] Thus, sensing applications of ring resonators can be realized by simply detecting spectral shifts of the optical resonant modes.[261,265] For example, the modes' positions shift to lower energies when the microtube wall is coated with Al_2O_3 monolayers using atomic layer deposition. Each Al_2O_3 layer with a thickness of ~0.9 Å leads to an average optical shift of 0.35 meV.[266] The tubular geometry of the rolled-up microtube resonator is especially suitable for sensing the refractive index evolution of a liquid. The small cross-sectional area of the microtube is particularly striking and allows analysis of fluid volumes in the range of femto-liters. Emission spectra of optical modes from a microtube with a diameter of ~9 μm in different liquids show remarkable shift (see Figure 14a) and are well-fitted by theoretical simulation as demonstrated in Figure 14b.[261] For a certain azimuthal number m, pronounced optical shifts of the modes to longer wavelengths are observed, and a maximum shift of more than 90 nm for $m = 48$ is determined when the refractive index is increased from 1 to 1.38, with the highest sensitivity of 425 nm/refractive index unit achieved in an optimized microtube resonator with subwavelength tube wall thickness.[261] Since the optical shift is determined by the evanescent field, the sensitivity can be further enhanced at longer wavelengths, which suggests great potential in integrated opto-fluidics.

The rolled-up technology presents a novel way to fabricate radial superlattices consisting of metal/oxide or metal/semiconductor bi-layers with a tunable layer thickness ratio and lattice constant,[267–269] where coupling of the plasmon polaritons to normal optical resonant modes exists.[270–272] Both theoretical and experimental results show that effective plasma frequency of the radial superlattice can be tuned over a broad range by changing the layer thickness ratio in good agreement with a metamaterial description.[272] In such structures, the electromagnetic field is radially channeled, exhibiting subwavelength imaging, and giving rise to the use of such structures as hyperlenses.[272] Furthermore, if the propagation of the electromagnetic field along the axial direction of this metamaterial microtube is considered, theoretical investigation suggests a dual effect of surface plasmon and classical waveguiding in the structure.[271] The ability to manipulate different materials and their combinations in rolled-up technology permits a feasible way to develop such structures experimentally. Combination of the sensing and waveguiding functions of rolled-up

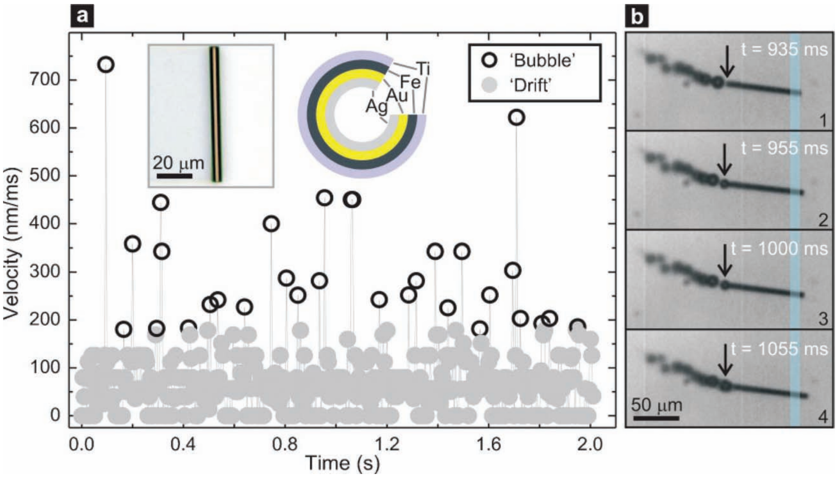

Figure 15. (a) Velocity of a rolled-up catalytic micro-engine as a function of time. Left inset shows an optical image of a single microtube and right inset a sketch of the tubular structure. (b) Selected video frames of a micro-engine at different stages of the motion. Reproduced from ref. [42].

microtubes has great potential in on-chip integrated analyzing systems.

5.4.2. Micro-engines

It is well known that catalysts such as Pt or Ag decompose H_2O_2 into O_2 and water. By employing rolled-up technology, those catalysts can be easily incorporated into the microtube on the inner side of the tube wall, as demonstrated in the inset of **Figure 15**a. An experimental result in Figure 15b exhibits an optical image of a rolled-up Ti/Fe/Au/Ag microtube.[42] The inner wall of the microtube thus decomposes H_2O_2 and produces gaseous O_2. The accumulation of the produced O_2 in the tubular cavity leads to the formation of O_2 bubbles. Due to imperfections in the tubular structure, the bubbles will be ejected in a certain direction from the larger opening,[273] and the corresponding recoiling force pushes the microtube in the opposite direction.[42] The optical images of the movement of the rolled-up microtube are displayed in Figure 15b, suggesting potential applications of microtubes as a catalytic micro-engines in a fuel liquid.[42] Detailed analyses of the video recording the movement proved that the micro-engine thrusts in repeated cycles, as reflected in the velocity-time plot in Figure 15b.[42] One can see distinct velocity peaks (black open circles) of up to 720 nm/ms, which are much higher than the drift motion at ~150 nm/ms (grey full circles) caused by background liquid flow. As displayed in Figure 15b, a cyclic geometry change from a "single tube" into "a single tube with an attached bubble" and vice versa causes the motion of the micro-engine at low Reynolds numbers.[274] The shape of the system changes between Frame 1 (tube without bubble) and 2 (tube with a bubble), causing a one step movement. Expansion of the bubble (Frame 3), which is still attached to the end of the tube, provides an additional step of movement. The bubble finally detaches from the tube (Frame 4), generating a further discrete movement. Once detached, the system is restored to the original shape (tube without bubble) and ready for the next motion cycle.[42]

Before the micro-engines can be put into real applications, its motion behaviors need to be clarified. Several factors influence the motion in terms of trajectory and speed.[275] Firstly, the asymmetry and opening of the microtube alter the interaction between the microtube and the O_2 bubbles, causing the micro-engines to move with different trajectories.[273] Secondly, the composition and concentration of the fuel liquid significantly affect the speed of the micro-engine.[275] In general, at relatively low H_2O_2 concentrations, the speed increases with H_2O_2 concentration.[275] Obviously, the speed should be determined by the O_2 production through a recoiling effect, and investigation phenomenally shows that the velocity of the micro-engine is almost equal to the product of the bubble radius and expelling frequency.[273] The increase in speed with high H_2O_2 concentrations is mainly due to the increased expulsion frequency. Adopting a surfactant in the liquid fuel also raises the speed of the micro-engine.[273] A Pt surface is inherently hydrophobic, and refrains from mixing with the aqueous fuel solution. A surfactant can effectively reduce the surface tension of the liquid and achieve better wetting of the Pt surface and thus accelerate the chemical reaction.[275] However, the speed is reduced in liquid with very high concentrations of the surfactant since the surfactant may occupy the chemically active sites of Pt, which in turn reduces the catalytic area of the micro-engine.[275] Thirdly, micro-engines accelerate in liquid fuel with elevated temperatures.[276] In the experimental investigation at physiological temperatures i.e. 37 °C, only 0.25% H_2O_2 is needed to propel the micro-engines.[276] One can see the motion of rolled-up catalytic micro-engines is rather complicated, involving chemical reactions and hydrodynamics. Recently, a simple model was presented to describe the dynamics of a micro-engine with linear trajectory, and it was found that the speed (v) can be estimated using the following equation:[277]

$$v = \frac{9nC_{H_2O_2} R_e L_e}{3R_b^2 + L R_b / \left(\ln\left(\frac{2L_e}{R_e}\right) - 0.72\right)}, \tag{3}$$

where R_e and L_e are the length and the radius of the microtube respectively, C_{H2O2} the H_2O_2 concentration, n the O_2 production rate, and R_b the bubble radius.

The controllability of the rolled-up micro-engine is also the focus of much research. Dynamic magnetic control is always the easiest way as long as a magnetic material is embedded into the rolled-up structure. The motion direction is determined by the magnetic field, and in the case of a rotating magnetic field, the motion can be localized into a circular trajectory.[273,275] Experiment shows that the localization radius decreases when the rotating frequency is increased.[273] The air-liquid interface is also useful in controlling the micro-engines,[275] and the micro-engines were observed to be trapped at the interface (which can be formed simply using a micro-object manipulated externally) by the meniscus-climbing effect. The balance between capillary and drag forces determines assembly and disassembly of the micro-engines, which therefore exemplifies a dynamic self-assembly behavior.[275] Very recently, researchers demonstrated control over the propulsion of micro-engines using a light source which induces a local decrease of the fuel and the surfactant concentrations, both of which contribute to the full switching off of the micro-engine.[278] This controllability is also wavelength-dependent: shorter wavelengths suppress the generation of bubbles more rapidly relative to longer wavelengths.[278]

For the most important application in cargo transportation and delivery, rolled-up catalytic micro-engines have shown the ability to transport polymer particles in a liquid.[275] By engaging a similar approach, animal cells and even single-strand DNA molecules can also be manipulated based on the selective binding and transport ability of bio-functionalized micro-engines, where the rapid movement of the micro-engine and corresponding fluid convection enables a rapid and selective isolation of cell, protein, or nucleic acid targets.[279–281] However, in bio-application, the concentration of H_2O_2 should be kept low. To achieve similar self-propelled motion, researchers functionalized a thin Au inner surface with self-assembled-monolayers where the catalase enzymes were covalently bonded.[275] Catalase can decompose millions of H_2O_2 molecules every second into H_2O and O_2 which propels the micro-engine to move with a speed 10 times higher than that of Pt-based micro-engine.[275] Therefore, this kind of micro-engine can work in very dilute H_2O_2 solutions, which will be of benefit to future applications in biology.

Self-propelled microtubes are not the only type of rolled-nanomembrane-based micro-engines. Recently, rolled nanobelts in the form of a micro-helix have been connected to a soft-magnetic head to resemble natural flagella. Experimental observation showed that this artificial bacterial flagella can be propelled and steered precisely in water by a low-strength rotating magnetic field.[282] The motion mechanism is completely different but as a kind of micro-engine the rotating micro-helix should have similar application potentials.

5.4.3. Cell Culture Scaffolds

Rolled-up microtubes offer the advantage of a uniform diameter, a good directionality and a two-dimensional confinement, which can be considered as an *in vitro* mimic of a vessel. Due to the difficulty in the experiment, investigation into this aspect has started just recently and as such only a few papers have been published so far.

Researchers have already used the rolled-up microtubes to practically guide *in vitro* growth of living cells within, and the results give clues as to the mechanical interaction between cells and microtubes.[283] The first attempt is based on the guided growth of yeast cells in the rolled-up SiO_x microtubes with an additional Al_2O_3 coating later.[283] These oxide microtubes provide an optically transparent container enabling in situ monitoring of the growth and the budding of yeast cells via conventional optical microscopy. Cell culture experiments have proved that as culture scaffolds, these oxide rolled-up microtubes demonstrate good bio-compatibility, because quantitative analyses showed that the reproduction behaviors are similar for yeast cells inside or outside the microtube and their doubling times (~100 min) are also comparable.[283] However, confinement within the tubular channels, especially in the case of those with smaller diameters, caused a rotation of cell pairs leading to different cell arrangements. In the microtubes with a diameter smaller than the cell size, the yeast cells are well aligned like a chain but their elongation is distinct. The cells in the small microtube were found to have a shrinkage in their volumes and this was ascribed to a nutrition shortage, indicating the bio-activities of the cells are suppressed although they are still alive.[283] However, as a single cell organism, the yeast cell in many ways does not resemble the situation in higher eukaryotes. Therefore, the investigation was extended by seeding primary mouse motor neurons and immortalised catecholaminergic cells on a substrate with microtube arrays to investigate the influence of topographical surface features on the growth and differentiation behavior of these cells.[284] The results showed that the microtubes and their arrays act as a platform for axon guidance with protruding cell extensions aligning in the direction of the microtubes and forming complex square-shaped grid-like neurite networks. Meanwhile, the cells growing inside the tubes demonstrated increased photoresistance.[284] The guided growth was very recently observed for neuron cells cultured on Si/SiGe rolled-up microtubes as well.[285] The microtube with a semiconductor nature resembles natural myelin both physically and electrically, and thus provides a confined contact with the axon membrane to insulate it from the extracellular solution.[285]

With the demonstrated micro-fluidic application of rolled-up microtubes,[240] the microtube culture scaffold can be incorporated with other optical or magnetic applications to form an integrated lab-in-a-tube system.[286]

5.4.4. Electrical Applications

Electrical characterization of rolled-up metal microtubes proves that the resistivity of the tube wall resembles that in bulk material.[40] In the case of semiconductor microtubes, researchers reported a linear *I-V* property and an increased resistance compared to the nanomembrane before release.[32] The increase in resistance was considered to be due to the added surface states on the new surface acting as charge traps, as we discussed in section 2.1.1. Generally, the electrical properties of a rolled-up nanomembrane should be similar to its counterpart as a free-standing nanomembrane and the surface states may play an important role.[287] The rolling behavior and the accompanying additional strain affect the energy band structure leading to band bending, but its influence on electric properties is negligible with respect to that from the surface states.[287] Furthermore, magnetoresistance measurements suggest that the electron transport in the rolled nanomembrane is anisotropically influenced by the magnetic field due to the unique cylindrical geometry.[288–290] In general, electric performance is lower in rolled-up microtubes, nevertheless, their unique geometries still have potential in some advanced applications.

As we know, the rolling behavior of the nanomembrane can produce an additional interface between the inside layer and the outside layer in between the windings upon contact.[20] If the layer is conductive, this contact can be used for electrical measurements,[291] which is quite useful in characterizing organic materials because most common deposition methods for metallic electrodes often have devastating effects on ultrathin molecular layers.[291] Several efforts have been made so far, for instance researchers have fabricated hybrid organic/inorganic heterojunctions from strained metal and/or semiconductor nanomembranes as electrodes using rolled-up technology, which is fully integrative on-chip. In this way, heterojunctions consisting of metal/self-assembled molecular layers/metal, and those consisting of semiconductor/self-assembled molecular layers/semiconductor have been created.[291] In the case of semiconductor contacts, a flexible control can be achieved by tuning the position of the Fermi level within the semiconductor band gap through the precise adjustment of dopant amount and density, but these contacts cannot be easily formed by other methods without destroying the organic molecules. The current approach thus has the ability of placing the electrode in intimate contact with the measured layer without damaging its intrinsic properties or affecting the overall junction stability and reproducibility by introducing pinholes and defects.[291] Moreover, the fabrication process is compatible with conventional photolithography, and thus several devices can be processed in parallel.

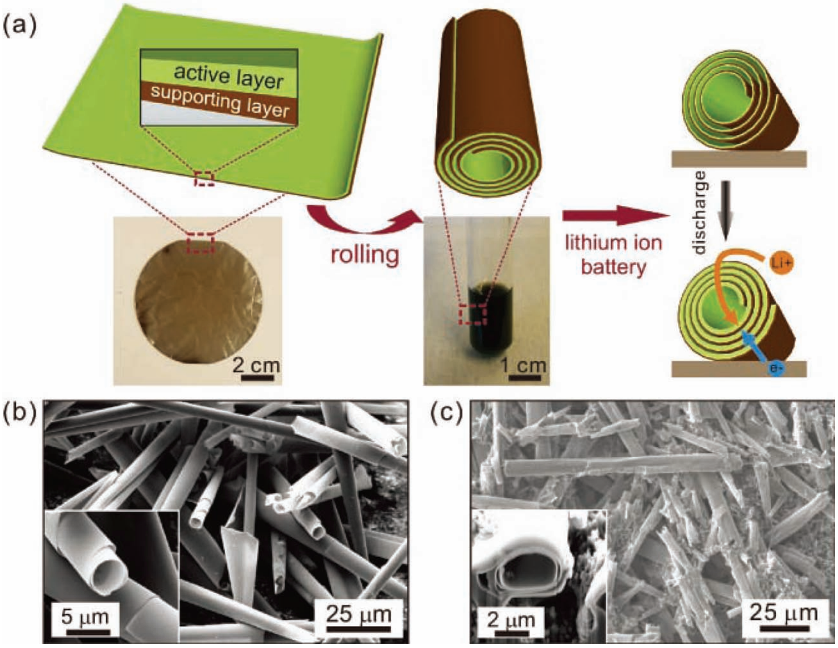

Figure 16. (a) Schematic illustration of the fabrication process of rolled-up RuO_2/C microtube electrodes. The photo shows the composite nanomembrane (50 nm RuO_2/15 nm C) on a photoresist sacrificial layer and the rolled-up microtube suspension in acetone. (b), (c) Scanning electron microscopy images of the rolled-up microtubes before (b) and after (c) mixing with polyvinylidene fluoride binder. The insets show enlarged images of the open ends. Reproduced from ref. [293].

Another field that rolled-up microtubes can be engaged in is energy storage because this approach can produce tubular structures almost two orders of magnitude smaller than their planar counterparts, and consequently, high density energy storage can be realized.[292] By rolling nanomembranes with materials possessing different functions, another advantage of rolled-up technology has been realized: a super-capacitor was fabricated with high performance characteristics such as a capacitance per footprint area of ~200 µF/cm^2 and specific energy of ~0.55 W·h/kg.[292] Moreover, the rolled-up microtubes were recently reported to have been used as electrode materials for lithium ion batteries. The proof-of-concept studies were based on ruthenium dioxide/carbon (RuO_2/C) bi-layer nanomembranes,[293] where RuO_2 is used as the active layer owing to its ability to reversibly store lithium by a conversion reaction,[294] and carbon is employed to serve as the supporting layer because of its high stability as an anode material in ion batteries and its reasonable electrical conductivity for charge separation.[295] During fabrication, bi-layer nanomembranes consisting of a 50 nm RuO_2 layer and a 15 nm C layer were deposited by sputtering on a photoresist sacrificial layer, as shown in the left panel of **Figure 16**a. The bi-layer nanomembranes were released and self-rolled after being immersed into acetone (middle panel of Figure 16a). The detailed morphology of the rolled-up microtube is shown in Figure 16b, where each microtube with diameter of ~5 µm presents an open end and a smooth tube wall that originates from the initially deposited bi-layer nanomembrane. Then, the microtubes were mixed with acetylene black and polyvinylidene fluoride to prepare a work electrode for battery cycling (right panel of Figure 16a). The morphology of the work electrode is shown in Figure 16c, consisting of microtubes with open ends.[293] Electrochemical characterization demonstrates that the fifteenth discharge/charge curves for the RuO_2/C microtubes still show a feature of RuO_2, and reach a discharge capacity of 830 mA·h/g and a coulombic efficiency of 99%. The values are much better than that of the RuO_2 powder as a reference sample although the two samples show similar behavior in the first cycle, which implies an enhanced lifetime and good reversibility of the RuO_2/C microtubes. The microtube electrode also shows high specific capacity at higher discharge/charge rates.[293] There are three factors contributing to the enhanced performance. Firstly, the relaxed strain of the tubular structure and the nanometer-thickness allow for enhanced tolerance to stress cracking. Secondly, the C supporting layer maintains the structural integrity during the conversion reaction which would otherwise break the homogeneity of the structure. Thirdly, the whole active layer adheres to the conductive supporting layer surface, which leads to good electrical contact.[293] It is believed that the employing of suitable materials, which should be easy to produce using rolled-up technology from polymers, may further improve the performance of the work electrode.

6. Summary and outlook

In this Review, we have summarized recent progress in the field of nanomembrane research, which is a rapidly expanding frontier in nanoscience and technology. Typically, the term "nanomembrane" refers to the quasi-two-dimensional structure with thickness between one to a few hundred nanometers and lateral dimensions at least one or two orders of magnitude larger and is isolated from its environment at both sides. Due to the direct compatibility with the methods and processes used in the conventional semiconductor industry, nanomembranes made out of groups IV and III-V semiconductors were investigated first and in the most detail. Tremendous efforts have been directed towards epitaxial nanomembranes because the composition and the strain inside can be precisely tuned via sophisticated experimental design, and theoretical studies also benefit from the ideal periodicity that exists in the lattice. With the rapid development of micro-/nanofabrication technology and fundamental research in nanoscience, more advanced materials are nowadays being investigated in the form of nanomembranes. Oxides, metals, and even organic materials have been successfully thinned by employing bottom-up (i.e. evaporation and spin-coating) and top-down (i.e. exfoliation or etching) approaches with high throughputs and yields, while the structure of the nanomembrane itself has also developed from single-layer to bi-layer or multi-layer, expanding the nanomembrane family.

The thickness of the nanomembranes is between the atomic scale and the macro scale and thus they present many unique properties very different from those exhibited on a macro scale. For instance, with greatly decreasing structural size, electronic properties are altered with the influence from surface/interface states and quantum confinement effect. Nanomembranes with novel opto-electronical and thermo-electrical properties have been disclosed and studied. Thinning also improves bendability and stretchability of the nanomembranes because the bending strain is significantly reduced in ultra-thin nanomembranes, and thus traditional inorganic semiconductor materials like Si have been found to become soft, enabling their use in bendable and stretchable electronics. By combining pre-defined shaping and following under-etching, freestanding nanomembranes are released. The strain-engineering of such freestanding nanomembranes causes them to be curved, bent or wrinkled, and interesting three-dimensional micro-/nanostructures can be architected by self-organization. Typical structures include wrinkled microchannels, rolled-up microtubes, and rolled-up microsprings, which possess unique geometries as well as new properties different from the constitutive materials in nanomembrane form. Preliminary applications in optics, chemistry, electronics, and biology have already been demonstrated.

The future of the nanomembranes lies in many aspects of fundamental science, engineering, and application potential. Fabrication of nanomembranes is expected to be expanded both in terms of materials and methodology by technological innovations over the coming years. Multi-layer nanomembranes and ultra-thin nanomembranes are the most promising structures. So far, fabrication of nanomembranes with thickness less than 10 nm is difficult except with the exfoliation of graphene, while the quantum confinement effect and surface/interface states in such cases should have paramount influence. The surface/interface deterministically affects the physical and chemical properties of nanomembranes while the underneath mechanism is worth further investigation. The relative studies are of importance in fundamental research, similar to those studies on quantum dots and wires. Moreover, this unique feature also predicts a sensing application for nanomembranes via surface functionalization. Introduction and tuning of strain in non-epitaxial nanomembranes are also worthy since precise control of strain status in such nanomembranes is so far difficult. More complicated self-organized three-dimensional structures produced by inherent stress can be fabricated by advanced strain engineering. Besides those novel applications summarized in this Review, we hope researchers can explore more amazing application potentials using curved or rolled nanomembranes. These devices as building blocks for a large integrative MEMS or NEMS can be easily integrated onto a chip using common techniques for integrated-circuit manufacturing, serving for fascinating applications in electronics, mechanics, fluidics, biology, and photonics.

Acknowledgements

This work is supported by the Natural Science Foundation of China (Nos. 61008029 and 51102049), Program for New Century Excellent Talents in University (No. NCET-10-0345), Shanghai Pujiang Program (No. 11PJ1400900), and "Shu Guang" project by Shanghai Municipal Education Commission and Shanghai Education Development Foundation.

Received: February 10, 2012

[1] L. B. Freund, S. Suresh, *Thin film materials: Stress, Defect Formation and Surface Evolution,*Cambridge University Press, New York, **2003**.
[2] J. A. Rogers, M. G. Lagally, R. G. Nuzzo, *Nature* **2011**, *477*, 45, and references therein.
[3] J. Matovic, Z. Jakšić, In: *Micro Electronic and Mechanical Systems,* V. Kordic, Ed., In-Tech, Vienna, **2009**.
[4] E. Kay, *Annu. Rev. Mater. Sci.* **1971**, *1*, 289.
[5] M. Ohring, *Materials science of thin films: deposition and structure* (2nd edition), Academic Press, San Diego, **2002**.
[6] R. C. Jaeger, *Introduction to Microelectronic Fabrication, second edition,*Prentice Hall, Upper Saddle River, New Jersey, **2002**.
[7] A. Y. Cho, J. R. Arthur, *Prog. Solid State Chem.* **1975**, *10*, 157.
[8] C. J. Brinker, G. W. Scherer, *Sol-Gel Science: The Physics and Chemistry of Sol-Gel Processing,*Academic Press, New York, **1990**.
[9] L. L. Hench, J. K. West, *Chem. Rev.* **1990**, *90*, 33.
[10] M. O'Donoghue, *A guide to man-made gemstones,*Van Nostrand Reinhold Company, New York, **1983**.
[11] R. Bacsa, P. Ravindranathan, J. P. Dougherty, *J. Mater. Res.* **1992**, *7*, 423.
[12] R. C. Xie, J. K. Shang, *J. Mater. Sci.* **2007**, *42*, 6583.
[13] M. Choucair, P. Thordarson, J. A. Stride, *Nat. Nanotechnol.* **2009**, *4*, 30.
[14] M. Stelter, H. Bombach, *Adv. Eng. Mater.* **2004**, *6*, 558.
[15] U. Mennicke, T. Salditt, *Langmuir* **2002**, *18*, 8172.
[16] S. Markutsya, C. Y. Jiang, Y. Pikus, V. V. Tsukruk, *Adv. Func. Mater.* **2005**, *15*, 771.
[17] C. Y. Jiang, M. E. McConney, S. Singamaneni, E. Merrick, Y. C. Chen, J. Zhao, L. Zhang, V. V. Tsukruk, *Chem. Mater.* **2006**, *18*, 2632.
[18] O. Moutanabbir, U. Gösele, *Annu. Rev. Mater. Res.* **2010**, *40*, 469.
[19] M. Pelliccione, T.-M. Lu, *Evolution of Thin FilmMorphology: Modeling and Simulations,*Springer-Verlag, New York, **2008**.

[20] G. S. Huang, Y. F. Mei, F. Cavallo, S. Baunack, E. Coric, T. Gemming, F. Bertram, J. Christen, R. K. Y. Fu, Paul K. Chu, O. G. Schmidt, *J. Appl. Phys.* **2009**, *105*, 016103.
[21] M. H. Huang, F. Cavallo, F. Liu, M. G. Lagally, *Nanoscale* **2011**, *3*, 96, and references therein.
[22] Y. F. Mei, S. Kiravittaya, M. Benyoucef, D. J. Thurmer, T. Zander, C. Deneke, F. Cavallo, A. Rastelli, O. G. Schmidt, *Nano Lett.* **2007**, *7*, 1676.
[23] Y.-J. Chen, J.-H. Hsu, H.-N. Lin, *Nanotechnology* **2005**, *16*, 1112.
[24] J.-X. Li, B.-R. Lu, Z. K. Shen, Z. C. Xu, H. Li, J. J. Wen, Z. D. Li, X.-P. Qu, Y.-F. Chen, Y. F. Mei, R. Liu, *Microelec. Eng.* **2011**, *88*, 1792.
[25] J. P. Colinge, *Silicon-on-Insulator technology: materials to VLSI,* Kluwer Academic Publishers, Norwell, **1991**.
[26] F. Cavallo, R. Songmuang, C. Ulrich, O. G. Schmidt, *Appl. Phys. Lett.* **2007**, *90*, 193120.
[27] F. Wang, Y. Shi, J. Liu, Y. Lu, S. Gu, Y. Zhang, *J. Electrochem. Soc.* **1997**, *144*, L37.
[28] N. Y. Jin-Phillipp, J. Thomas, M. Kelsch, Ch. Deneke, R. Somuang, O. G. Schmidt, *Appl. Phys. Lett.* **2006**, *88*, 033113.
[29] V. Ya. Prinz, V. A. Seleznev, A. K. Gutakovsky, A. V. Chehovskiy, V. V. Preobrazhenskii, M. A. Putyato, T. A. Gavrilova, *Phys. E.* **2000**, *6*, 828.
[30] L. Dong, L. Zhang, D. J. Bell, D. Grützmacher, B. J. Nelson, *J. Phys. Conf. Ser.* **2007**, *61*, 257.
[31] D. Grützmacher, L. Zhang, L. Dong, D. J. Bell, B. J. Nelson, A. Prinz, E. Ruh, *Microelectron. J.* **2008**, *39*, 478.
[32] F. Cavallo, R. Somuang, O. G. Schmidt, *Appl. Phys. Lett.* **2008**, *93*, 143113.
[33] O. G. Schmidt, N. Schmarje, Ch. Deneke, C. Müller, N. Y. Phillipp, *Adv. Mater.* **2001**, *13*, 756.
[34] R. Somuang, A. Rastelli, S. Mendach, O. G. Schmidt, *Appl. Phys. Lett.* **2007**, *90*, 091905.
[35] R. Somuang, Ch. Deneke, O. G. Schmidt, *Appl. Phys. Lett.* **2006**, *89*, 223109.
[36] S. Mendach, R. Somuang, S. Kiravittaya, A. Rastelli, M. Benyoucef, O. G. Schmidt, *Appl. Phys. Lett.* **2006**, *88*, 111120.
[37] G. D Cole, Y. Bai, M. Aspelmeyer, E. A. Fitzgerald, *Appl. Phys. Lett.* **2010**, *96*, 261102.
[38] H. Kim, C. Kim, M. R. Yu, H.-S. Kim, R. H. Blick, *J. Appl. Phys.* **2010**, *108*, 074307.
[39] B. A. Ganji, B. Y. Majlis, *Microsyst. Technol.* **2010**, *16*, 1803.
[40] Y. V. Nastaushev, V. Ya. Prinz, S. N. Svitasheva, *Nanotechnology* **2005**, *16*, 908.
[41] A. Bagolini, L. Pakula, T. L. M. Scholtes, H. T. M. Pham, P. J. French, P. M. Sarro, *J. Micromech. Microeng.* **2002**, *12*, 385.
[42] Y. F. Mei, G. S. Huang, A. A. Solovev, E. Bermúdez Ureña, I. Mönch, F. Ding, T. Reindl, R. K. Y. Fu, P. K. Chu, O. G. Schmidt, *Adv. Mater.* **2008**, *20*, 4085.
[43] G. S. Huang, S. Kiravittaya, V. A. Bolaños Quiñones, F. Ding, M. Benyoucef, A. Rastelli, Y. F. Mei, O. G. Schmidt, *Appl. Phys. Lett.* **2009**, *94*, 141901.
[44] M. M. Hawkeye, M. J. Brett, *J. Vac. Sci. Technol. A* **2007**, *25*, 1317.
[45] Y.-P. Zhao, D.-X. Ye, G.-C. Wang, T.-M. Lu, *Nano Lett.* **2002**, *1*, 351.
[46] F. Liu, M. T. Umlor, L. Shen, J. Weston, W. Eads, J. A. Barnard, G. J. Mankey, *J. Appl. Phys.* **1999**, *85*, 5486.
[47] F. Cavallo, M. G. Lagally, *Soft Matter* **2010**, *6*, 439, and references therein.
[48] S. A. Scott, M. G. Lagally, *J. Phys. D: Appl. Phys.* **2007**, *40*, R75, and references therein.
[49] M. G. Lagally, *MRS Bull.* **2007**, *32*, 57.
[50] M. Harb, W. Peng, G. Sciaini, C. T. Hebeisen, R. Ernstorfer, M. A. Eriksson, M. G. Lagally, S. G. Kruglik, R. J. D. Miller, *Phys. Rev. B* **2009**, *79*, 094301.
[51] C. Euaruksakul, F. Chen, B. Tanto, C. S. Ritz, D. M. Paskiewicz, F. J. Himpsel, D. E. Savage, Z. Liu, Y. G. Yao, F. Liu, M. G. Lagally, *Phys. Rev. B* **2009**, *80*, 115323.
[52] S. Seo, C. Euaruksakul, D. E. Savage, M. G. Lagally, P. G. Evans, *Phys. Rev. B* **2010**, *81*, 041302.
[53] A. M. Kiefer, D. M. Paskiewicz, A. M. Clausen, W. R. Buchwald, R. A. Soref, M. G. Lagally, *ACS Nano* **2011**, *5*, 1179.
[54] M. H. Huang, C. S. Ritz, B. Novakovic, D. C. Yu, Y. Zhang, F. Flack, D. E. Savage, P. G. Evans, I. Knezevic, F. Liu, M. G. Lagally, *ACS Nano* **2009**, *3*, 721.
[55] M. M. Roberts, L. J. Klein, D. E. Savage, M. Friesen, G. K. Celler, M. A. Eriksson, M. G. Lagally, *Nat. Mater.* **2006**, *5*, 388.
[56] H. Ko, K. Takei, R. Kapadia, S. Chuang, H. Fang, P. W. Leu, K. Ganapathi, E. Plis, H. S. Kim, S.-Y. Chen, M. Madsen, A. C. Ford, Y.-L. Chueh, S. Krishna, S. Salahuddin, A. Javey, *Nature* **2010**, *468*, 286.
[57] Z. H. Lu, D. J. Lockwood, J. M. Baribeau, *Nature* **1995**, *378*, 258.
[58] B. Legrand, V. Agache, J. P. Nys, V. Senez, D. Stievenard, *Appl. Phys. Lett.* **2000**, *76*, 3271.
[59] W. Liu, M. Asheghi, *Appl. Phys. Lett.* **2004**, *84*, 3819.
[60] P. P. Zhang, E. Tevaarwerk, B.-N. Park, D. E. Savage, G. K. Celler, I. Knezevic, P. G. Evans, M. A. Eriksson, M. G. Lagally, *Nature* **2006**, *439*, 703.
[61] P. P. Zhang, E. P. Nordberg, B.-N. Park, G. K. Celler, I. Knezevic, P. G. Evans, M. A. Eriksson, M. G. Lagally, *New J. Phys.* **2006**, *8*, 200.
[62] T. Shinada, S. Okamoto, T. Kobayashi, I. Ohdomari, *Nature* **2005**, *437*, 1128.
[63] S. A. Scott, W. N. Peng, A. M. Kiefer, H. Q. Jiang, I. Knezevic, D. E. Savage, M. A. Eriksson, M. G. Lagally, *ACS Nano* **2009**, *3*, 1683.
[64] F. Chen, E. B. Ramayya, C. Euaruksakul, G. J. Himpsel, G. K. Celler, B. J. Ding, I. Knezevic, M. G. Lagally, *ACS Nano* **2010**, *4*, 2466.
[65] X. F. Zhao, S. A. Scott, M. H. Huang, W. N. Peng, A. M. Kiefer, F. S. Flack, D. E. Savage, M. G. Lagally, *Nanoscale Res. Lett.* **2011**, *6*, 402.
[66] T. Takahagi, A. Ishitani, H. Kuroda, Y. Nagasawa, *J. Appl. Phys.* **1991**, *69*, 803.
[67] M. Gräf, M. Grundner, R. Schulz, *J. Vac. Sci. Technol. A* **1989**, *7*, 808.
[68] L. Ling L, S. Kuwabara, T. Abe, F. Shimura, *J. Appl. Phys.* **1993**, *73*, 3018.
[69] H. Angermann, W. Henrion, M. Rebien, A. Röseler, *Appl. Surf. Sci.* **2004**, *235*, 322.
[70] D. Watanabe, A. En, S. Nakamura, M. Suhara, T. Okumura, *Appl. Surf. Sci.* **2003**, *216*, 24.
[71] R. Schlaf, R. Hinogami, M. Fujitani, S. Yae, Y. Nakato, *J. Vac. Sci. Technol. A* **1999**, *17*, 164.
[72] M. Liehr, C. M. Greenlief, M. Offenberg, S. R. Kasi, *J. Vac. Sci. Technol. A* **1990**, *8*, 2960.
[73] M. V. Fischetti, S. E. Laux, *J. Appl. Phys.* **1996**, *80*, 2234.
[74] A. Tiberj, B. Fraisse, C. Blanc, S. Contreras, J. Camassel, *J. Phys.: Condens. Matter* **2002**, *14*, 13411.
[75] C. Euaruksakul, Z. W. Li, F. Zheng, F. J. Himpsel, C. S. Ritz, B. Tanto, D. E. Savage, X. S. Liu, M. G. Lagally, *Phys. Rev. Lett.* **2008**, *101*, 147403.
[76] P. Feng, I. Mönch, S. Harazim, G. S. Huang, Y. F. Mei, O. G. Schmidt, *Nano Lett.* **2009**, *9*, 3453.
[77] M. Hundhausen, L. Ley, *Phys. Rev. B* **1985**, *32*, 6655.
[78] S. M. Sze, *miconductor Devices: Physics and Technology,* Wiley, New York, **2002**.
[79] D. V. Lang, R. A. Logan, *Phys. Rev. Lett.* **1977**, *39*, 635.
[80] H. J. Queisser, D. E. Theodorou, *Phys. Rev. Lett.* **1979**, *43*, 401.
[81] M. Freitag, M. Radosavljevic, Y. Zhou, A. T. Johnson, W. F. Smith, *Appl. Phys. Lett.* **2001**, *79*, 3326.

[82] S. Heinze, J. Tersoff, R. Martel, V. Derycke, J. Appenzeller, Ph. Avouris, *Phys. Rev. Lett.* **2002**, *89*, 106801.
[83] Y. Ahn, J. Dunning, J. Park, *Nano Lett.* **2005**, *5*, 1367.
[84] W. Mönch, *Rep. Prog. Phys.* **1990**, *53*, 221.
[85] G. K. Celler, S. Cristolovreanu, *J. App. Phys.* **2003**, *93*, 4955.
[86] D. Connelly, P. J. Clifton, *J. Appl. Phys.* **2008**, *103*, 074506.
[87] M. Freitag, J. C. Tsang, A. Bol, D. Yuan, J. Liu, Ph. Avouris, *Nano Lett.* **2007**, *7*, 2037.
[88] P. Feng, I. Mönch, G. S. Huang, S. Harazim, E. J. Smith, Y. F. Mei, O. G. Schmidt, *Adv. Mater.* **2010**, *22*, 3667.
[89] G. J. Snyder, E. S. Toberer, *Nat. Mater.* **2008**, *7*, 105.
[90] F. J. DiSalvo, *Science* **1999**, *285*, 703.
[91] L. D. Hicks, M. S. Dresselhaus, *Phys. Rev. B* **1993**, *47*, 16631.
[92] D. G. Cahill, W. K. Ford, K. E. Goodson, G. D. Mahan, A. Majumdar, H. J. Maris, R. Merlin, S. R. Phillpot, *J. Appl. Phys.* **2003**, *93*, 793.
[93] J. Y. Tang, H.-T. Wang, D. H. Lee, M. Fardy, Z. Y. Huo, T. P. Russell, P. D. Yang, *Nano Lett.* **2010**, *10*, 4279.
[94] J.-K. Yu, S. Mitrovic, D. Tham, J. Varghese, J. R. Heath, *Nat. Nanotechnol.* **2010**, *5*, 718.
[95] Z. Aksamija, I. Knezevic, *Phys. Rev. B* **2010**, *82*, 045319.
[96] C. Bera, N. Mingo, S. Volz, *Phys. Rev. Lett.* **2010**, *104*, 115502.
[97] M. Zhang, S. Fang, A. A. Zakhidov, S. B. Lee, A. E. Aliev, C. D. Williams, K. R. Atkinson, R. H. Baughman, *Science* **2005**, *309*, 1215.
[98] A. Ikeda, Y. Tsuchiya, T. Konishi, S. Ogasawara, J. Kikuchi, *Chem. Mater.* **2005**, *17*, 4018.
[99] H. Watanabe, T. Kunitake, *Adv. Mater.* **2007**, *19*, 909.
[100] H. Lee, K. Neville, *Handbook of Epoxy Resins,*McGraw-Hill, New York, **1967**.
[101] I. Park, H.-G. Peng, D. W. Gidley, S. Xue, T. J. Pinnavaia, *Chem. Mater.* **2006**, *18*, 650.
[102] P. B. Messersmith, E. P. Giannelis, *Chem. Mater.* **1994**, *6*, 1719.
[103] E. Amerio, M. Sangermano, G. Malucelli, A. Priola, B. Voit, *Polymer* **2005**, *46*, 11241.
[104] J. Choi, S. G. Kim, R. M. Laine, *Macromolecules* **2004**, *37*, 99.
[105] H. Watanabe, E. Muto, T. Ohzono, A. Nakao, T. Kunitake, *J. Mater. Chem.* **2009**, *19*, 2425.
[106] R. Vendamme, S.-Y. Onoue, A. Nakao, T. Kunitake, *Nat. Mater.* **2006**, *5*, 494.
[107] H. Watanabe, A. Fujimoto, A. Takahara, *Soft Matter* **2011**, *7*, 1856.
[108] C. Y. Jiang, S. Markutsya, Y. Pikus, V. V. Tsukruk, *Nat. Mater.* **2004**, *3*, 721.
[109] L. H. Sperling, *Polymeric Multicomponent Materials 37*, Wiley, New York, **1997**.
[110] Y. C. Rao, R. Jin, C. A. Mirkin, *Science* **2002**, *297*, 1536.
[111] C. Y. Jiang, W. Y. Lio, V. V. Tsukruk, *Phys. Rev. Lett.* **2005**, *95*, 115503.
[112] C. Y. Jiang, S. Markutsya, V. V. Tsukruk, *Langmuir* **2004**, *20*, 882.
[113] D. Zimnisky, C. Y. Jiang, J. Xu, Z. Q. Lin, L. Zhang, V. V. Tsukruk, *Langmuir* **2007**, *23*, 10176.
[114] Y. Bao, Q. A. N. Luu, C. K. Lin, J. M. Schloss, P. S. May, C. Y. Jiang, *J. Mater. Chem.* **2010**, *20*, 8356.
[115] N. M. R. Peres, *Rev. Mod. Phys.* **2010**, *82*, 2673.
[116] K. S. Novoselov, A. K. Geim, S. V. Morozov, D. Jiang, Y. Zhang, S. V. Dubonos, I. V. Grigorieva, A. A. Firsov, *Science* **2004**, *306*, 666.
[117] K. S. Novoselov, D. Jiang, T. Booth, V. V. Khotkevich, S. V. Morozov, A. K. Geim, *Proc. Natl. Acad. Sci. U. S. A.* **2005**, *102*, 10451.
[118] T. J. Booth, P. Blake, R. R. Nair, D. Jiang, E. W. Hill, U. Bangert, A. Bleloch, M. Gass, K. S. Novoselov, M. I. Katsnelson, A. K. Geim, *Nano Lett.* **2008**, *8*, 2442.
[119] C. W. J. Beenakker, *Rev. Mod. Phys.* **2008**, *80*, 1337.
[120] M. J. Allen, V. C. Tung, R. B. Kaner, *Chem. Rev.* **2010**, *110*, 132.
[121] S. Stankovich, D. A. Dikin, G. H. B. Dommett, K. M. Kohlhaas, E. J. Zimney, E. A. Stach, R. D. Piner, S. T. Nguyen, R. S. Ruoff, *Nature* **2006**, *442*, 282.
[122] J. S. Wu, W. Pisula, K. Mullen, *Chem. Rev.* **2007**, *107*, 718.
[123] K. S. Kim, *Nature* **2009**, *457*, 706.
[124] C. Berger, Z. M. Song, X. B. Li, X. S. Wu, N. Brown, C. Naud, D. Mayou, T. B. Li, J. Hass, A. N. Marchenkov, E. H. Conrad, P. N. First, W. A. de Heer, *Science* **2006**, *312*, 1191.
[125] K. S. Novoselov, A. K. Geim, S. V. Morozov, D. Jiang, M. I. Katsnelson, I. V. Grigorieva, S. V. Dubonos, A. A. Firsov, *Nature* **2005**, *438*, 197.
[126] K. S. Novoselov, E. McCann, S. V. Morozov, V. I. Fal'ko, M. I. Katsnelson, U. Zeitler, D. Jiang, F. Schedin, A. K. Geim, *Nat. Phys.* **2006**, *2*, 177.
[127] C. G. Lee, X. D. Wei, J. W. Kysar, J. Hone, *Science* **2008**, *321*, 385.
[128] J. A. Rogers, *Nat. Nanotechnol.* **2008**, *3*, 254.
[129] F. Cavallo, D. S. Grierson, K. T. Turner, M. G. Lagally, *ACS Nano* **2011**, *5*, 5400.
[130] F. Ding, R. Singh, J. D. Plumhof, T. Zander, V. Křápek, Y. H. Chen, M. Benyoucef, V. Zwiller, K. Dörr, G. Bester, A. Rastelli1, O. G. Schmidt, *Phys. Rev. Lett.* **2010**, *104*, 067405.
[131] J. R. Sánchez-Pérez, C. Boztug, F. Chen, F. F. Sudradjat, D. M. Paskiewicz, R. B. Jacobson, M. G. Lagally, R. Paiella, *Proc. Natl. Acad. Sci. U. S. A.* **2011**, *108*, 18893.
[132] J. Song, H. Jiang, Y. Huang, J. A. Rogers, *J. Vac. Sci. Technol. A* **2009**, *27*, 1107.
[133] Y. G. Sun, J. A. Rogers, *Adv. Mater.* **2007**, *19*, 1897.
[134] A. J. Beca, J.-H. Ahn, Y. G. Sun, M. A. Meitl, E. Menard, H.-S Kim, W. M. Choi, D.-H. Kim, Y. Huang, J. A. Rogers, *Angew. Chem. Int. Ed.* **2008**, *47*, 5524.
[135] J. A. Rogers, T. Someya, Y. G. Huang, *Science* **2010**, *327*, 1603, and references therein.
[136] D.-H. Kim, J. A. Rogers, *Adv. Mater.* **2008**, *20*, 4887.
[137] D.-H. Kim, J. L. Xiao, J. Z. Song, Y. G. Huang, J. A. Rogers, *Adv. Mater.* **2010**, *22*, 2108.
[138] D.-H. Kim, N. Lu, R. Ma, Y.-S. Kim, R.-H. Kim, S. Wang, J. Wu, S. M. Won, H. Tao, A. Islam, K. J. Yu, T.-I. Kim, R. Chowdhury, M. Ying, L. Xu, M. Li, H.-J. Chung, H. Keum, M. McCormick, P. Liu, Y.-W. Zhang, F. G. Omenetto, Y. Huang, T. Coleman, J. A. Rogers, *Science* **2011**, *333*, 838.
[139] F. Garnier, R. Hajlaoui, A. Yassar, P. Srivastava, *Science* **1994**, *265*, 1684.
[140] G. H. Gelinck, H. E. A. Huitema, E. Van Veenendaal, E. Cantatore, L. Schrijnemakers, J. B. P. H. Van Der Putten, T. C. T. Geuns, M. Beenhakkers, J. B. Giesbers, B. Huisman, E. J. Meijer, E. M. Benito, F. J. Touwslager, A. W. Marsman, B. J. E. van Rens, D. M. de Leeuw, *Nat. Mater.* **2004**, *3*, 106.
[141] T. Someya, Y. Kato, T. Sekitani, S. Lba, Y. Noguchi, Y. Murase, H. Kawaguchi, T. Sakurai, *Proc. Natl. Acad. Sci. U. S. A.* **2005**, *102*, 12321.
[142] P. F. Baude, D. A. Ender, M. A. Haase, T. W. Kelley, D. V. Muyres, S. D. Theiss, *Appl. Phys. Lett.* **2003**, *82*, 3964.
[143] H.-C. Yuan, J. Y. Shin, G. X. Qin, L. Sun, P. Bhattacharya, M. G. Lagally, G. K. Celler, Z. Q. Ma, *Appl. Phys. Lett.* **2009**, *94*, 013102.
[144] A. J. Baca, J.-H. Ahn, Y. Sun, M. A. Meitl, E. Menard, H.-S. Kim, W. M. Choi, D.-H. Kim, Y. Huang, J. A. Rogers, *Angew. Chem. Int. Ed.* **2008**, *47*, 2.
[145] A. Ghaffari, A. Hosseini, X. C. Xu, D. Kwong, H. Subbaraman, R. T. Chen, *Opt. Express* **2010**, *18*, 20086.
[146] G. X. Qin, H.-C. Yuan, G. K. Celler, J. G. Ma, Z. Q. Ma, *Appl. Phys. Lett.* **2010**, *97*, 233110.
[147] H.-C. Yuan, M. M. Kelly, D. E. Savage, M. G. Lagally, G. K. Celler, Z. Q. Ma, *IEEE T. Electron Dev.* **2008**, *55*, 810.
[148] R.-H. Kim, M.-H. Bae, D. G. Kim, H. Cheng, B. H. Kim, D.-H. Kim, M. Li, J. Wu, F. Du, H.-S. Kim, S. Kim, D. Estrada, S. W. Hong, Y. Huang, E. Pop, J. A. Rogers, *Nano Lett.* **2011**, *11*, 3881.
[149] X. Hu, P. Krull, B. de Graff, K. Dowling, J. A. Rogers, W. J. Arora, *Adv. Mater.* **2011**, *23*, 2933.

[150] J. Yoon, L. Li, A. V. Semichaevsky, J. H. Ryu, H. T. Johnson, R. G. Nuzzo, J. A. Rogers, *Nat. Commun.* **2011**, *2*, 343.
[151] S.-I. Park, A.-P. Le, J. Wu, Y. Huang, X. Li, J. A. Rogers, *Adv. Mater.* **2010**, *22*, 3062.
[152] M. Q. Xue, Z. Xie, L. S. Zhang, X. L. Ma, X. L. Wu, Y. G. Guo, W. G. Song, Z. B. Li, T. B. Cao, *Nanoscale* **2011**, *3*, 2703.
[153] X. Feng, B. D. Yang, Y. Liu, Y. Wang, C. Dagdeviren, Z. Liu, A. Carlson, J. Li, Y. Huang, J. A. Rogers, *ACS Nano* **2011**, *5*, 3326.
[154] J. Xiao, A. Carlson, Z. J. Liu, Y. Huang, H. Jiang, J. A. Rogers, *Appl. Phys. Lett.* **2008**, *93*, 013109.
[155] X. L. Wang, H. Hu, Y. D. Shen, X. C. Zhou, Z. Zhen, *Adv. Mater.* **2011**, *23*, 3090.
[156] P. Gorrn, W. Z. Cao, S. Wagner, *Soft Matter* **2011**, *7*, 7177.
[157] H. Q. Jiang, D.-Y. Khang, J. Z. Song, Y. G. Sun, Y. G. Huang, J. A. Rogers, *Proc. Natl. Acad. Sci. U. S. A.* **2007**, *104*, 15607.
[158] H. C. Ko, M. P. Stoykovich, J. Z. Song, V. Malyarchuk, W. M. Choi, C.-J. Yu, J. B. Geddes III, J. L. Xiao, S. D. Wang, Y. G. Huang, J. A. Rogers, *Nature* **2008**, *454*, 748.
[159] I. Jung, J. Xiao, V. Malyarchuk, C. Lub, M. Li, Z. Liu, J. Yoon, Y. Huang, J. A. Rogers, *Proc. Natl. Acad. Sci. U. S. A.* **2011**, *108*, 1788.
[160] H. S. Wang, Q. Li, K. Liu, C. L. Chien, *Appl. Phys. Lett.* **1999**, *74*, 2212.
[161] K. K. Choi, T. Taniyama, Y. Yamazaki, *J. Appl. Phys.* **2001**, *90*, 6145.
[162] Y. F. Chen, J. McCord, J. Freudenberger, R. Kaltofen, O. G. Schmidt, *J. Appl. Phys.* **2009**, *105*, 07C302.
[163] M. N. Baibich, J. M. Broto, A. Fert, F. Nguyen Van Dau, F. Petroff, P. Eitenne, G. Creuzet, A. Friederich, J. Chazelas, *Phys. Rev. Lett.* **1988**, *61*, 2472.
[164] G. Binasch, P. Grünberg, F. Saurenbach, W. Zinn, *Phys. Rev. B* **1989**, *39*, 4828.
[165] G. A. Prinz, *Science* **1998**, *282*, 1660.
[166] S. S. P. Parkin, *Appl. Phys. Lett.* **1996**, *69*, 3092.
[167] F. Yan, G. Xue, F. Wan, *J. Mater. Chem.* **2002**, *12*, 2606.
[168] Y.-F. Chen, Y. F. Mei, R. Kaltofen, I. Mönch, J. Schumann, J. Freudenberger, H.-J. Klauβ, O. G. Schmidt, *Adv. Mater.* **2008**, *20*, 3224.
[169] R. Coehoorn, *Phys. Rev. B* **1991**, *44*, 9331.
[170] J. Mathon, A. Umerski, M. Villeret, *Phys. Rev. B* **1997**, *55*, 14378.
[171] M. Melzer, D. Makarov, A. Calvimontes, D. Karnaushenko, S. Baunack, R. Kaltofen, Y. F. Mei, O. G. Schmidt, *Nano Lett.* **2011**, *11*, 2522.
[172] I. Mönch, D. Makarov, R. Koseva, L. Baraban, D. Karnaushenko, C. Kaiser, K.-F. Arndt, O. G. Schmidt, *ACS Nano* **2011**, *5*, 7436.
[173] A. H. C. Neto, F. Guinea, N. M. R. Peres, K. S. Novoselov, A. K. Geim, *Rev. Mod. Phys.* **2009**, *81*, 109.
[174] Z. H. Ni, T. Yu, Y. H. Lu, Y. Y. Wang, Y. P. Feng, Z. X. Shen, *ACS Nano* **2008**, *2*, 2301.
[175]H. Tomori, A. Kanda, H. Goto, Y. Ootuka, K. Tsukagoshi, S. Moriyama, E. Watanabe, D. Tsuya, *Appl. Phys. Express* **2011**, *4*, 075102.
[176] A. K. Geim, K. S. Novoselov, *Nat. Mater.* **2007**, *6*, 183.
[177] M. Y. Han, B. Ozyilmaz, Y. B. Zhang, P. Kim, *Phys. Rev. Lett.* **2007**, *98*, 206805.
[178] H. Min, B. Sahu, S. K. Banerjee, A. H. MacDonald, *Phys. Rev. B* **2007**, *75*, 155115.
[179] D. C. Elias, R. R. Nair, T. M. G. Mohiuddin, S. V. Morozov, P. Blake, M. P. Halsall, A. C. Ferrari, D. W. Boukhvalov, M. I. Katsnelson, A. K. Geim, K. S. Novoselov, *Science* **2009**, *323*, 610.
[180] H. Miyazaki, K. Tsukagoshi, A. Kanda, M. Otani, S. Okada, *Nano Lett.* **2010**, *10*, 3888.
[181] E. D. Minot, Y. Yaish, V. Sazonova, J.-Y. Park, M. Brink, P. L. McEuen, *Phys. Rev. Lett.* **2003**, *90*, 156401.
[182] F. Guinea, M. I. Katsnelson, A. K. Geim, *Nat. Phys.* **2010**, *6*, 30.
[183] P. Liu, Y. W. Zhang, *Appl. Phys. Lett.* **2009**, *94*, 231912.
[184] E. Mariani, F. von Oppen, *Phys. Rev. Lett.* **2008**, *100*, 076801.
[185] P. Koskinen, *Appl. Phys. Lett.* **2011**, *99*, 013105.
[186] O. Frank, G. Tsoukleri, J. Parthenios, K. Papagelis, I. Riaz, R. Jalil, K. S. Novoselov, C. Galiotis, *ACS Nano* **2010**, *4*, 3131.
[187] T. M. G. Mohiuddin, A. Lombardo, R. R. Nair, A. Bonetti, G. Savini, R. Jalil, N. Bonini, D. M. Basko, C. Galiotis, N. Marzari, K. S. Novoselov, A. K. Geim, A. C. Ferrari, *Phys. Rev. B* **2009**, *79*, 205433.
[188] Y. C. Cheng, Z. Y. Zhu, G. S. Huang, U. Schwingenschlögl, *Phys. Rev. B* **2011**, *83*, 115449.
[189] F. Ding, H. X. Ji, Y. H. Chen, A. Herklotz, K. Dörr, Y. F. Mei, A. Rastelli, O. G. Schmidt, *Nano Lett.* **2010**, *10*, 3453.
[190] J. E. Proctor, E. Gregoryanz, K. S. Novoselov, M. Lotya, J. N. Coleman, M. P. Halsall, *Phys. Rev. B* **2009**, *80*, 073408.
[191] D. C. Yu, F. Liu, *Nano Lett.* **2007**, *7*, 3046.
[192] F. Liu, M. G. Lagally, J. Zang, *MRS Bull.* **2009**, *34*, 190.
[193] Z. N. Qi, F. P. Zhao, X. Z. Zhou, Z. H. Sun, H. S. Park, H. G. Wu, *Nanotechnology* **2010**, *21*, 265702.
[194] J. Zheng, H. T. Liu, B. Wu, Y. L. Guo, T. Wu, G. Yu, Y. Q. Liu, D. B. Zhu, *Adv. Mater.* **2011**, *23*, 2460.
[195] J. Zheng, H. T. Liu, B. Wu, Y. L. Guo, T. Wu, G. Yu, Y. Q. Liu, D. B. Zhu, *Nano Res.* **2011**, *4*, 705.
[196] E. Erdogan, I. Popov, G. Seifert, *Phys. Rev. B* **2011**, *83*, 245417.
[197] E. Cerda, L. Mahadevan, *Phys. Rev. Lett.* **2003**, *90*, 074302.
[198] J. Genzer, J. Groenewold, *Soft Matter* **2006**, *2*, 310.
[199] Y. F. Mei, S. Kiravittaya, S. Harazim, O. G. Schmidt, *Mat. Sci. Eng. R* **2010**, *70*, 209.
[200] N. Bowden, S. Brittain, A. G. Evans, J. W. Hutchinson, G. W. Whitesides, *Nature* **1998**, *393*, 146.
[201] M. C. Cross, P. C. Hohenberg, *Rev. Mod. Phys.* **1993**, *65*, 851.
[202] C. H. Lu, H. Möhwald, A. Fery, *Soft Matter* **2007**, *3*, 1530.
[203] C. M. Stafford, C. Harrison, K. L. Beers, A. Karim, E. J. Amis, M. R. Vanlandingham, H.-C. Kim, W. Volksen, R. D. Miller, E. E. Simonyi, *Nat. Mater.* **2004**, *3*, 545.
[204] Y. Karade, S. A. Pihan, W. H. Brünger, A. Dietzel, R. Berger, K. Graf, *Langmuir* **2009**, *25*, 3108.
[205] K. Efimenko, M. Rackaitis, E. Manias, A. Vaziri, L. Mahadevan, J. Genzer, *Nat. Mater.* **2005**, *4*, 293.
[206] B. Sanii, A. M. Smith, R. Butti, A. M. Brozell, A. N. Parikh, *Nano Lett.* **2008**, *8*, 866.
[207] N. Bowden, W. T. S. Huck, K. E. Paul, G. M. Whitesides, *Appl. Phys. Lett.* **1999**, *75*, 2557.
[208] S. Chung, J. H. Lee, M.-W. Moon, J. Han, R. D. Kamm, *Adv. Mater.* **2008**, *20*, 3011.
[209] Y. F. Mei, D. J. Thurmer, F. Cavallo, S. Kiravittaya, O. G. Schmidt, *Adv. Mater.* **2007**, *19*, 2124.
[210] A. Malachias, Y. F. Mei, R. K. Annabattula, C. Deneke, P. R. Onck, O. G. Schmidt, *ACS Nano* **2008**, *2*, 1715.
[211] P. Cendula, S. Kiravittaya, Y. F. Mei, Ch. Deneke, O. G. Schmidt, *Phys. Rev. B* **2009**, *79*, 085429.
[212] J. M. Torres, C. M. Stafford, B. D. Vogt, *ACS Nano* **2009**, *3*, 2677.
[213] C. M. Stafford, B. D. Vogt, C. Harrison, D. Julthongpiput, R. Huang, *Macromolecules* **2006**, *39*, 5095.
[214] D. Tahk, H. H. Lee, D.-Y. Khang, *Macromolecules* **2009**, *42*, 7079.
[215] J. Y. Chung, T. Q. Chastek, M. J. Fasolka, H. W. Ro, C. M. Stafford, *ACS Nano* **2009**, *3*, 844.
[216] J. C. Tsang, P. M. Mooney, F. Dacol, J. O. Chu, *J. Appl. Phys.* **1994**, *75*, 8098.
[217] C. Pryor, M. E. Pistol, L. Samuelson, *Phys. Rev. B* **1997**, *56*, 10404.
[218] M. Grundmann, *Appl. Phys. Lett.* **2003**, *83*, 2444.
[219] L. D. Landau, L. Lifshitz, *Theory of Elasticity* (3rd edition), Pergamon, New York, **1986**.
[220] C. G. Van de Walle, *Phys. Rev. B* **1989**, *39*, 1871.
[221] D. Huh, K. L. Mills, X. Zhu, M. A. Burns, M. D. Thouless, S. Takayama, *Nat. Mater.* **2007**, *6*, 424.

[222] N. Douville, D. Huh, S. Takayama, *Anal. Bioanal. Chem.* **2008**, *391*, 2395.
[223] S. M. Harazim, P. Feng, S. Sanchez, C. Deneke, Y. F. Mei, O. G. Schmidt, *Nanoscale Res. Lett.* **2011**, *6*, 215.
[224] O. G. Schmidt, K. Eberl, *Nature* **2001**, *410*, 168.
[225] W.-P. Huang, H. H. Cheng, A. I. Fedorchenko, A.-B. Wang, *Appl. Phys. Lett.* **2007**, *91*, 053103.
[226] R. Huang, Z. Suo, *J. Appl. Phys.* **2002**, *91*, 1135.
[227] A. I. Fedorchenko, A.-B. Wang, V. I. Mashanov, W.-P. Huang, H. H. Cheng, *Appl. Phys. Lett.* **2006**, *89*, 043119.
[228] F. Liu, M. G. Lagally, J. Zang, *MRS Bull.* **2009**, *34*, 190.
[229] P. G. Evans, D. S. Tinberg, M. M. Roberts, M. G. Lagally, Y. Xiao, B. Lai, Z. Cai, *Appl. Phys. Lett.* **2005**, *87*, 073112.
[230] S. V. Golod, V. Ya. Prinz, P. Wägli, L. Zhang, O. Kirfel, E. Deckhardt, F. Glaus, C. David, D. Grützmacher, *Appl. Phys. Lett.* **2004**, *84*, 1.
[231] D. J. Bell, L. X. Dong, B. J. Nelson, *Nano Lett.* **2006**, *6*, 725.
[232] L. Zhang, E. Deckhardt, A. Weber, C. Schönenberger, D. Grützmacher, *Nanotechnology* **2006**, *16*, 655.
[233] L. Zhang, E. Ruh, D. Grützmacher, *Nano Lett.* **2006**, *6*, 1311.
[234] S. V. Golod, V. Ya. Prinz, V. I. Mashanov, A. K. Gutakovsky, *Semicond. Sci. Technol.* **2001**, *16*, 181.
[235] H. Seidel, L. Csepregi, A. Heuberger, H. Baumgärtel, *J. Electrochem. Soc.* **1990**, *137*, 3612.
[236] Y. L. Shen, S. Suresh, I. A. Blech, *J. Appl. Phys.* **1996**, *80*, 1388.
[237] S. Timoshenko, *J. Opt. Soc. Am.* **1925**, *11*, 233.
[238] M. H. Huang, C. Boone, M. Roberts, D. E. Savage, M. G. Lagally, N. Shaji, H. Qin, R. H. Blick, J. A. Nairn, F. Liu, *Adv. Mater.* **2005**, *17*, 2860.
[239] D. J. Bell, Y. Sun, L. Zhang, L. X. Dong, B. J. Nelson, D. Grützmacher, *Sens. Actuators A: Phys.* **2006**, *130–131*, 54.
[240] D. J. Thurmer, Ch. Deneke, Y. F. Mei, O. G. Schmidt, *Appl. Phys. Lett.* **2006**, *89*, 223507.
[241] P. O. Vaccaro, K. Kubota, T. Aida, *Appl. Phys. Lett.* **2001**, *78*, 2852.
[242] J. Q. Hu, Y. Bando, J. H. Zhan, M. Y. Liao, D. Golberg, X. L. Yuan, T. Sekiguchi, *Appl. Phys. Lett.* **2005**, *87*, 113107.
[243] M. F. Doerner, W. D. Nix, *Crit. Rev. Solid State Mater. Sci.* **1988**, *14*, 225.
[244] J. Zang, M. H. Huang, F. Liu, *Phys. Rev. Lett.* **2007**, *98*, 146102.
[245] V. Luchnikov, O. Sydorenko, M. Stamm, *Adv. Mater.* **2005**, *17*, 1177.
[246] K. Kumar, B. Nandan, V. Luchnikov, E. Bhoje Gowd, M. Stamm, *Langmuir* **2009**, *25*, 7667.
[247] V. Luchnikov, K. Kumar, M. Stamm, *J. Micromech. Microeng.* **2008**, *18*, 035041.
[248] S. Zakharchenko, E. Sperling, L. Ionov, *Biomacromolecules* **2011**, *12*, 2211.
[249] C. Müller, M. S. Khatri, C. Deneke, S. Fähler, Y. F. Mei, E. Bermúdez Ureña, O. G. Schmidt, *Appl. Phys. Lett.* **2009**, *94*, 102510.
[250] D. K. Armani, T. J. Kippenberg, S. M. Spillane, K. J. Vahala, *Nature* **2003**, *421*, 925.
[251] K. J. Vahala, *Nature* **2003**, *424*, 839.
[252] H. Zhu, I. M. White, J. D. Suter, M. Zourob, X. Fan, *Anal. Chem.* **2007**, *79*, 930.
[253] I. M. White, H. Oveys, X. Fan, T. L. Smith, J. Zhang, *Appl. Phys. Lett.* **2006**, *89*, 191106.
[254] C. Monat, P. Domachuk, B. Eggleton, *Nat. Photonics* **2007**, *1*, 106.
[255] T. Kipp, H. Welsch, Ch. Strelow, Ch. Heyn, D. Heitmann, *Phys. Rev. Lett.* **2006**, *96*, 077403.
[256] F. Li, Z. T. Mi, S. Vicknesh, *Opt. Lett.* **2009**, *34*, 2915.
[257] F. Li, Z. T. Mi, *Opt. Exp.* **2009**, *17*, 19933.
[258] Ch. Strelow, H. Rehberg, C. M. Schultz, H. Welsch, Ch. Heyn, D. Heitmann, T. Kipp, *Phys. Rev. Lett.* **2008**, *101*, 127403.
[259] Ch. Strelow, C. M. Schultz, H. Rehberg, H. Welsch, Ch. Heyn, D. Heitmann, T. Kipp, *Phys. Rev. B* **2007**, *76*, 045303.
[260] G. S. Huang, S. Kiravittaya, V. A. Bolaños Quiñones, F. Ding, M. Benyoucef, A. Rastelli, Y. F. Mei, O. G. Schmidt, *Appl. Phys. Lett.* **2009**, *94*, 141901.
[261] G. S. Huang, V. A. Bolaños Quiñones, F. Ding, S. Kiravittaya, Y. F. Mei, O. G. Schmidt, *ACS Nano* **2010**, *4*, 3123.
[262] M. Hosoda, T. Shihaki, *Appl. Phys. Lett.* **2007**, *90*, 181107.
[263] Ch. Strelow, M. Sauer, S. Fehringer, T. Korn, C. Schüller, A. Stemmann, Ch. Heyn, D. Heitmann, T. Kipp, *Appl. Phys. Lett.* **2009**, *95*, 221115.
[264] K. Dietrich, Ch. Strelow, C. Schliehe, C. Heyn, A. Stemmann, S. Schwaiger, S. Mendach, A. Mews, H. Weller, D. Heitmann, T. Kipp, *Nano Lett.* **2010**, *10*, 627.
[265] A. Bernardi, S. Kiravittaya, A. Rastelli, R. Songmuang, D. J. Thurmer, M. Benyoucef, O. G. Schmidt, *Appl. Phys. Lett.* **2008**, *93*, 094106.
[266] V. A. Bolaños Quiñones, G. S. Huang, J. D. Plumhof, S. Kiravittaya, A. Rastelli, Y. F. Mei, O. G. Schmidt, *Opt. Lett.* **2009**, *34*, 2345.
[267] Ch. Deneke, N.-Y. Jin-Phillipp, I. Loa, O. G. Schmidt, *Appl. Phys. Lett.* **2004**, *84*, 4475.
[268] Ch. Deneke, U. Zschieschang, H. Klauk, O. G. Schmidt, *Appl. Phys. Lett.* **2006**, *89*, 263110.
[269] Ch. Deneke, W. Sigle, U. Eigenthaler, P. A. van Aken, G. Schütz, O. G. Schmidt, *Appl. Phys. Lett.* **2007**, *90*, 263107.
[270] A. Rottler, M. Bröll, S. Schwaiger, D. Heitmann, S. Mendach, *Opt. Lett.* **2011**, *36*, 1240.
[271] E. J. Smith, Z. Liu, Y. F. Mei, O. G. Schmidt, *Nano Lett.* **2010**, *10*, 1.
[272] S. Schwaiger, M. Bröll, A. Krohn, A. Stemmann, C. Heyn, Y. Stark, D. Stickler, D. Heitmann, S. Mendach, *Phys. Rev. Lett.* **2009**, *102*, 163903.
[273] A. A. Solovev, Y. F. Mei, E. B. Urena, G. S. Huang, O. G. Schmidt, *Small* **2009**, *5*, 1688.
[274] E. M. Purcell, *Am. J. Phys.* **1977**, *45*, 3.
[275] Y. F. Mei, A. A. Solovev, S. Sanchez, O. G. Schmidt, *Chem. Soc. Rev.* **2011**, *40*, 2109, and references therein.
[276] S. Sanchez, A. N. Ananth, V. M. Fomin, M. Viehrig, O. G. Schmidt, *J. Am. Chem. Soc.* **2011**, *133*, 14860.
[277] J. X. Li, G. S. Huang, M. M. Ye, M. L. Li, R. Liu, Y. F. Mei, *Nanoscale* **2011**, *3*, 5083.
[278] A. A. Solovev, E. J. Smith, C. C. Bof Bufon, S. Sanchez, O. G. Schmidt, *Angew. Chem. Int. Ed.* **2011**, *50*, 10875.
[279] S. Balasubramanian, D. Kagan, C. J. Hu, S. Campuzano, M. Jesus Lobo-Castañon, N. Lim, D. Y. Kang, M. Zimmerman, L. F. Zhang, J. Wang, *Angew. Chem. Int. Ed.* **2011**, *50*, 4161.
[280] D. Kagan, S. Campuzano, S. Balasubramanian, F. Kuralay, G.-U. Flechsig, J. Wang, *Nano Lett.* **2011**, *11*, 2083.
[281] J. Orozco, S. Campuzano, D. Kagan, M. Zhou, W. Gao, J. Wang, *Anal. Chem.* **2011**, *83*, 7962.
[282] L. Zhang, J. J. Abbott, L. X. Dong, K. E. Peyer, B. E. Kratochvil, H. X. Zhang, C. Bergeles, B. J. Nelson, *Nano Lett.* **2009**, *9*, 3663.
[283] G. S. Huang, Y. F. Mei, D. J. Thurmer, E. Coric, O. G. Schmidt, *Lab Chip* **2009**, *9*, 263.
[284] S. Schulze, G. S. Huang, M. Krause, D. Aubyn, V. A. Bolaños Quiñones, C. K. Schmidt, O. G. Schmidt, *Adv. Eng. Mater.* **2010**, *12*, B558.
[285] M. R. Yu, Y. Huang, J. Ballweg, H. Shin, M. H. Huang, D. E. Savage, M. G. Lagally, E. W. Dent, R. H. Blick, J. C. Williams, *ACS Nano* **2011**, *5*, 2447.
[286] E. J. Smith, S. Schulze, S. Kiravittaya, Y. F. Mei, S. Sanchez, O. G. Schmidt, *Nano Lett.* **2011**, *11*, 4037.
[287] N. V. Demarina, D. A. Grützmacher, *Appl. Phys. Lett.* **2011**, *98*, 192109.
[288] K.-J. Friedland, R. Hey, H. Kostial, A. Riedel, K. H. Ploog, *Phys. Rev. B* **2007**, *75*, 045347.

[289] N. Shaji, H. Qin, R. H. Blick, L. J. Kein, C. Deneke, O. G. Schmidt, *Appl. Phys. Lett.* **2007**, *90*, 042101.

[290] A. B. Vorob'ev, K.-J. Friedland, H. Kostial, R. Hey, U. Jahn, E. Wiebicke, Ju. S. Yukecheva, V. Ya. Prinz, *Phys. Rev. B* **2007**, *75*, 205309.

[291] C. C. Bof Bufon, J. D. A. Espinoza, D. J. Thurmer, M. Bauer, Ch. Deneke, U. Zschieschang, H. Klauk, O. G. Schmidt, *Nano Lett.* **2011**, *11*, 3727.

[292] C. C. Bof Bufon, J. D. Cojal González, D. J. Thurmer, D. Grimm, M. Bauer, O. G. Schmidt, *Nano Lett.* **2010**, *10*, 2506.

[293] H.-X. Ji, X.-L. Wu, L.-Z. Fan, C. Krien, I. Fiering, Y.-G. Guo, Y. F. Mei, O. G. Schmidt, *Adv. Mater.* **2010**, *22*, 4591.

[294] O. Delmer, P. Balaya, L. Kienle, J. Maier, *Adv. Mater.* **2008**, *20*, 501.

[295] J. W. Long, B. Dunn, D. R. Rolison, H. S. White, *Chem. Rev.* **2004**, *104*, 4463.